JACS
JOURNAL OF THE AMERICAN CHEMICAL SOCIETY

ARTICLE

pubs.acs.org/JACS

Identifying Guanosine Self Assembly at Natural Isotopic Abundance by High-Resolution ^{1}H and ^{13}C Solid-State NMR Spectroscopy

Amy L. Webber,[†,∥] Stefano Masiero,[‡] Silvia Pieraccini,[‡] Jonathan C. Burley,[§] Andrew S. Tatton,[†] Dinu Iuga,[†] Tran N. Pham,[†,⊥] Gian Piero Spada,[‡] and Steven P. Brown*[,†]

[†]Department of Physics, University of Warwick, Coventry CV4 7AL, United Kingdom

[‡]Dipartimento di Chimica Organica A. Mangini, Alma Mater Studiorum—Università di Bologna, Via San Giacomo 11, 40126 Bologna, Italy

[§]Boots Science Building, School of Pharmacy, University of Nottingham, University Park, Nottingham NG7 2RD, United Kingdom

Supporting Information

ABSTRACT: By means of the ^{1}H chemical shifts and the proton—proton proximities as identified in ^{1}H double-quantum (DQ) combined rotation and multiple-pulse spectroscopy (CRAMPS) solid-state NMR correlation spectra, ribbon-like and quartet-like self-assembly can be identified for guanosine derivatives without isotopic labeling for which it was not possible to obtain single crystals suitable for diffraction. Specifically, characteristic spectral fingerprints are observed for dG(C10)$_2$ and dG(C3)$_2$ derivatives, for which quartet-like and ribbon-like self-assembly has been unambiguously identified by ^{15}N refocused INADEQUATE spectra in a previous study of ^{15}N-labeled derivatives (Pham, T. N.; et al. *J. Am. Chem. Soc.* **2005**, *127*, 16018). The NH ^{1}H chemical shift is observed to be higher (13—15 ppm) for ribbon-like self-assembly as compared to 10—11 ppm for a quartet-like arrangement, corresponding to a change from NH···N to NH···O intermolecular hydrogen bonding. The order of the two NH$_2$ ^{1}H chemical shifts is also inverted, with the NH$_2$ proton closest in space to the NH proton having a higher or lower ^{1}H chemical shift than that of the other NH$_2$ proton for ribbon-like as opposed to quartet-like self-assembly. For the dG(C3)$_2$ derivative for which a single-crystal diffraction structure is available, the distinct resonances and DQ peaks are assigned by means of gauge-including projector-augmented wave (GIPAW) chemical shift calculations. In addition, ^{14}N—^{1}H correlation spectra obtained at 850 MHz under fast (60 kHz) magic-angle spinning (MAS) confirm the assignment of the NH and NH$_2$ chemical shifts for the dG(C3)$_2$ derivative and allow longer range through-space N···H proximities to be identified, notably to the N7 nitrogens on the opposite hydrogen-bonding face.

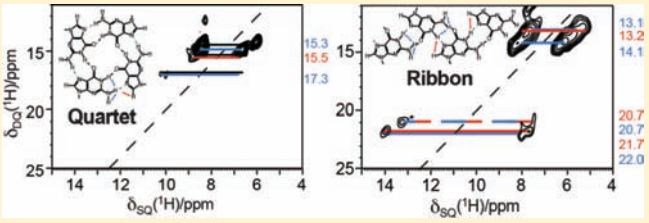

INTRODUCTION

Building upon their importance in biological systems, guanosine derivatives have been shown to exhibit a rich supramolecular chemistry in organic solutions, on surfaces and in the solid state.[1−3] Specifically, in 1995, Gottarelli et al. showed that quartet formation (see Figure 1a) occurs in organic solvents in the presence of metal ions for the deoxyguanosine derivative dG(C10)$_2$ (**1**),[4] while Davis et al. demonstrated analogous behavior for an isoguanosine derivative.[5] For **1**, well-organized yet different supramolecular assemblies were observed depending on the relative guanosine to metal ion molar ratio, as characterized by solution-state NMR, notably NOE experiments.[6,7] Pulse-field gradient diffusion NMR experiments have also been applied to characterize such supramolecular assemblies,[8−10] while the exchange of K^+, Na^+, and NH_4^+ cations has been followed using ^{1}H and ^{15}N solution-state NMR.[11] In the solid state, single-crystal X-ray diffraction structures of the stacking into quartets for a 5′-Me$_2$-*t*-BuSi-2′,3′,-di-*O*-isopropylidene guanosine derivative with a range of cations, Cs^+, K^+, Ba^{2+}, Pb^{2+}, and Sr^{2+}, have been presented;[12−16] the cation environment in such complexes has also been probed by ^{23}Na, ^{39}K, and ^{87}Rb solid-state NMR.[17−20] Single-crystal X-ray diffraction structures showing the stacking into pentamers of the analogous isoguanosine derivative with Cs^+ ions have also been reported.[21,22]

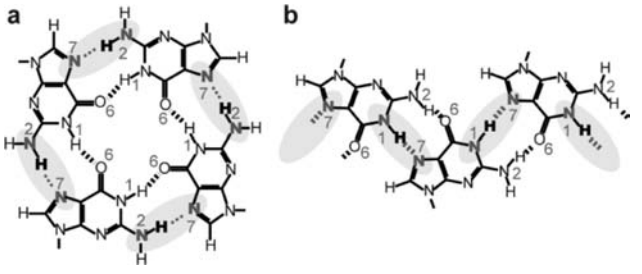

Figure 1. Formation of (a) quartet and (b) ribbon supramolecular structures by guanine, characterized by (a) N2—H···N7 and (b) N1—H···N7 intermolecular hydrogen bonding.

Received: July 13, 2011
Published: October 28, 2011

Recently, Rivera and co-workers have shown that fine control over the specific assembly of quartets can be achieved by tuning or changing the solvent composition for guanosines with a phenyl substituent at the C8 position,[23−25] while Meijer and co-workers have shown that Coulombic interactions between the separated cation and anion and solvent are also important in determining the exhibited self-assembly of guanosine quartets into 8-, 12-, 16-, or 24-mer structures.[26] The specificity for particular anions or cations of such guanosine quartet self-assembled structures is suggesting applications for ion extraction, e.g., for Cl^- or Ra^{2+}.[27,28] Moreover, Sreenivasachary and Lehn have shown that different propensity for self-assembly and thus gelation can be exploited in a combinatorial chemistry approach for component selection in the generation of constitutional dynamic hydrogels.[29]

In the absence of metal ions, **1** has been shown to self-assemble into ribbon-like structures in organic solvents,[30] thus forming liquid-crystalline phases,[31] with the transformation over time from a ribbon with a dipole moment to one without having been observed in $CDCl_3$ by solution-state NMR.[32] While it has not been possible to obtain a diffraction structure for the longer chain derivative **1**, an X-ray single-crystal diffraction structure for $dG(C3)_2$ (**2**) reveals the former type (i.e., with a dipole moment) of ribbon-like self-assembly (see Figure 1b),[33] as observed in the crystal structure of guanine monohydrate.[34] Similar ribbon-like self-assembly is observed in crystal structures presented by Araki and co-workers for a guanosine derivative with three Me_2-*t*-BuSi− substituents[35] and deoxyguanosine derivatives with two Ph_2-*t*-BuSi− or two Pr^i_3Si substituents,[36] with longer chain alkylsilyl derivatives having been shown to self-assemble into supramolecular films[37] or supramolecular vesicles composed of two-dimensional hydrogen-bonded sheets.[38]

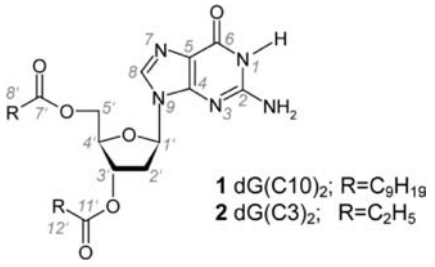

Interestingly, Sessler et al. presented a single-crystal X-ray diffraction structure for a guanosine derivative substituted at the C8 position with dimethylaniline,[39] showing quartet formation and, thus, that a templating metal cation is not a prerequisite for quartet formation. A similar observation was made in solution by Giorgi et al. for a 8-Br-substituted guanosine derivative, while circular dichroism and solution-state NMR suggest helical self-assembly for C10-substituted deoxyguanosine, inosine, and guanosine derivatives with an 8-oxo group.[40,41] On surfaces, guanosine ribbon-like and helical/quartet self-assembly has been observed by SFM and STM.[32,40,42,43] Nikan and Sherman have shown that guanosine-linked cavitands also exhibit guanosine quartets in the absence of metal ions.[44]

The rich self-assembly exhibited by guanosines is leading to the demonstration of a diverse range of nanostructures. In the presence of metal ions to template guanosine quartet formation, architectures such as nanotubes formed by a calix[4]arene guanosine,[45] anion-bridged nanosheets,[46] a membrane film,[47] and a star polymer[48] have been observed, while Barboiu and co-workers have shown how an organic−inorganic hybrid exhibiting an ion-channel-like columnar architecture can be formed by the self-organization of silicon-substituted guanosine quadruplexes and ureidocrown ethers.[49] Moreover, Davis and co-workers synthesized a guanosine derivative that has been demonstrated to function as a transmembrane transporter of sodium ions,[50] while forming a conjugate with bile acid or subsequent modification of carbamate to urea leads to formation of large and stable pores that would allow transport of larger biomolecules.[51,52]

1 has been used to fill the gap between nanocontacts obtained by electron-beam lithography, so as to produce devices with interesting electrical properties, namely, they are photoconductive,[53] and when the gap between the contacts is smaller than 100 nm, they act as a rectifier.[54,55] **1** has also been used for biophotonic applications[56] and shown to constitute a molecular electronic device with rectifying properties when conjugated to a wide band gap GaN semiconductor.[57]

Following the observation by Ghoussoub and Lehn that the reversible interconversion between a gel-forming ordered guanine-quartet structure and a disordered guanine solution can be achieved through cation release and binding using a cryptand,[58] Pieraccini et al. demonstrated the reversible interconversion between quartet and ribbon self-assembly for **1** by likewise using a cryptand for cation capture, with cation release being controlled by addition of acid to protonate a bridgehead nitrogen of the cryptand.[59] This has been exploited to switch spin−spin interactions in free-radical-substituted guanosines,[60,61] or to switch between supramolecular nanowire-like self-assemblies in oligothiophene-substituted guanosines,[62] or to achieve solvent-induced switching in terthiophene-substituted guanosines,[63] or for light-activated switching between ribbon and quartet self-assembly in a guanosine derivative carrying a vinylbenzene moiety.[64]

The chemist's ingenuity in exploiting hydrogen-bonding and aromatic $\pi-\pi$ interactions to produce a rich and diverse range of self-assembled guanosine structures is currently in contrast to the paucity of atomic-level solid-state characterization that exists for such nanostructures. Only in a few cases of short-chain derivatives noted above[12−16,21,22,35,36] has it been possible to obtain single-crystal X-ray diffraction structures. The purpose of this paper is to demonstrate that specific modes of self-assembly can be identified by solid-state NMR spectra obtained for guanosine derivatives without isotopic labeling, i.e., at natural abundance (1.1%) in ^{13}C.

Pham et al. have shown that ^{15}N refocused INADEQUATE[65−67] solid-state NMR spectra of ^{15}N-labeled **1** and **2** allow unambiguous identification of distinct intermolecular hydrogen bonding that is characteristic of different self-assembly into a quartet-like or ribbon-like arrangement (see Figure 1).[68] Specifically, the spectra exhibit double-quantum (DQ) peaks that are due to pairs of ^{15}N nuclei with a hydrogen-bond-mediated $^{2h}J_{NN}$ coupling.[68−72] For **2** (recrystallized from THF/H_2O), N1···N7 intermolecular hydrogen bonding is observed, as expected for the ribbon self-assembly (see Figure 1b) observed in the crystal structure.[33] For samples of **1** recrystallized from ethanol, two different polymorphs were identified: for one polymorph N1···N7 hydrogen bonding was observed as for the ribbon self-assembly of **2**, while a second polymorph (that forms more readily under recrystallization from ethanol and is the one analyzed in this paper) exhibited N2···N7 hydrogen bonding, as observed in a G-quartet (see Figure 1a). Note that both a quartet and a helical self-assembly can arise from N2···N7 intermolecular hydrogen bonding, and hence, the ^{15}N refocused INADEQUATE cannot distinguish

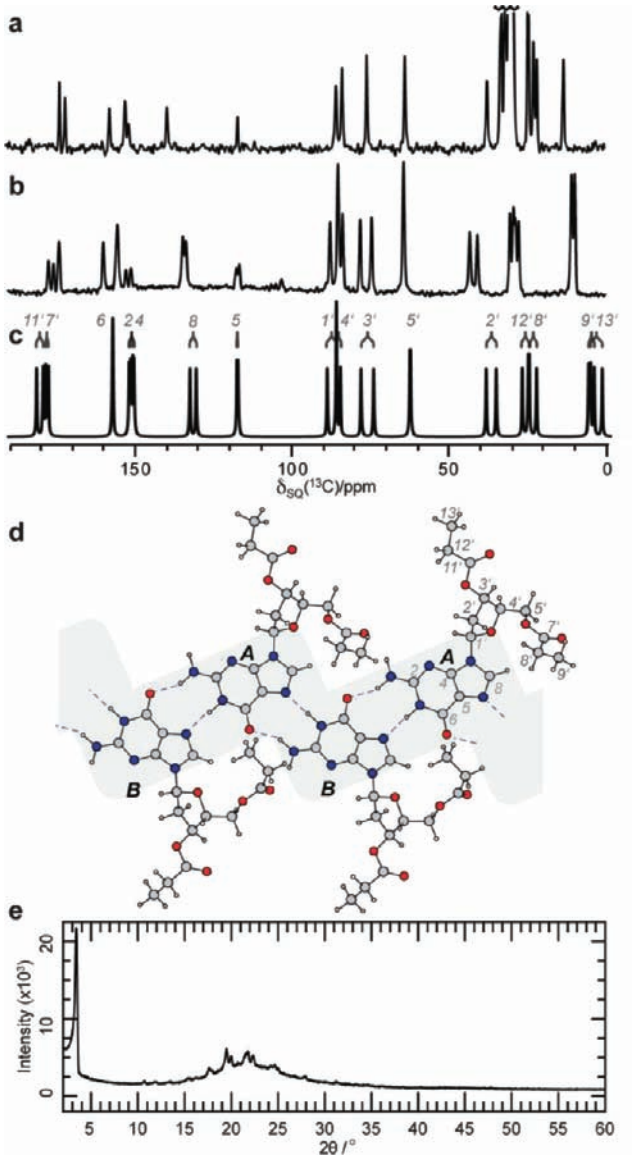

Figure 2. ^{13}C NMR spectra of (a) **1** and (b and c) **2**. (a and b) ^{13}C (150 MHz) CP MAS (12.5 kHz) NMR spectra. (a) Overlapped resonances of the multiple CH_2 groups around 20−30 ppm have been truncated so as to emphasize the resonances at larger chemical shift values. (c) Computed GIPAW ^{13}C chemical shifts as determined for the geometrically optimized (CASTEP) crystal structure of **2**, convoluted with 50 Hz Lorentzian line broadening and with site assignments shown. (d) Representation of the geometrically optimized (CASTEP) crystal structure of **2** with dashed lines, indicating the N1H···N7, N2H···O6 hydrogen-bonding interactions of the ribbon structure. The two distinct molecules of the asymmetric unit cell (A, B) are identified along with the carbon atom site labels. (e) Powder X-ray diffraction pattern of **1**.

between the two cases: in this paper, the notation "quartet-like" is used to address this ambiguity.

This paper presents ^{1}H and ^{13}C solid-state NMR spectra obtained for guanosine derivatives in the absence of metal ions and at natural isotopic abundance. Considering first the previously characterized deoxyguanosine dG(C10)$_2$ (**1**) and dG(C3)$_2$ (**2**) derivatives, ^{1}H and ^{13}C solid-state NMR signatures are identified that then allow the type of self-assembly in the solid state to be determined for four other guanosine derivatives for which it has not been possible to obtain single crystals suitable for X-ray diffraction: G(C3)$_3$ (**3**), G(C10)$_3$ (**4**), 8BrG(C10)$_3$ (**5**), and GaceC10 (**6**). The two-dimensional surface structure of Langmuir−Blodgett films formed by **1**, **4**, and **6**, as probed by AFM, has recently been described.[73] Derivatives **5** and **6** have been previously characterized by ^{1}H solution-state NMR in $CDCl_3$ and shown to exhibit quartet-like (**5**)[40] or ribbon-like (**6**)[33] self-assembly in the absence of metal ions.

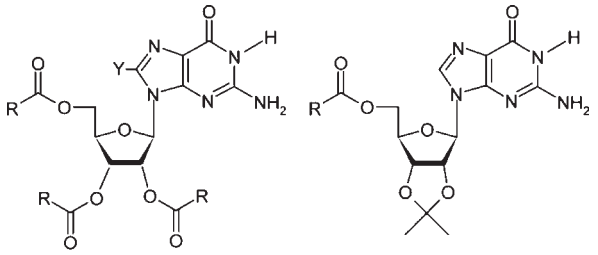

3 G(C3)$_3$; R=C_2H_5 Y=H **6** GaceC10; R=C_9H_{19}
4 G(C10)$_3$; R=C_9H_{19} Y=H
5 8BrG(C10)$_3$; R=C_9H_{19} Y=Br

RESULTS AND DISCUSSION

^{13}C CP MAS NMR of dG(C10)$_2$ (1) and dG(C3)$_2$ (2). The workhorse ^{13}C CP MAS experiment is particularly useful for identifying the number of distinct molecules in the asymmetric unit cell.[74] Comparing the ^{13}C CP MAS spectra of the deoxyguanosine derivatives, dG(C10)$_2$ (**1**) and dG(C3)$_2$ (**2**), shown in Figure 2a and 2b, a doubling of the number of observed resonances is evident for **2**. This is in agreement with the X-ray diffraction single-crystal structure of **2**,[33] shown in Figure 2d, where the two independent molecules in the asymmetric unit cell are identified. For comparison, a simulated spectrum based on ^{13}C chemical shifts calculated using the GIPAW[75−77] method for a geometrically optimized crystal is shown in Figure 2c. Good agreement between the experimental and the calculated chemical shifts for the CASTEP-optimized crystal structure is noted (see further discussion in section S1 in the Supporting Information), although, as is commonly observed with GIPAW calculations, experimental chemical shifts with low ppm values (i.e., CH_2 and CH_3 alkyl resonances) are underestimated by calculation, while those with high ppm values (i.e., carbonyl resonances here) are overestimated.[78−80]

It is interesting to note that the ^{13}C line widths are narrower for **1** as compared to **2** (full-width at half-maximum height, FWHMH, equals 51 and 85 Hz (average of the two resonances) for the C3′ sugar resonances), suggesting a well-ordered structure. In spite of this, it has to date not been possible to determine the crystal structure of **1** by X-ray diffraction. A powder X-ray diffraction pattern of **1** is shown in Figure 2e: the intensity is observed to drop off rather rapidly as a function of increasing scattering angle, which points toward molecular disorder within the lattice that is likely to be dynamic in nature (associated with the long alkyl chains). We note other examples of published solid-state NMR spectra for organic molecules with long alkyl chains, where good resolution is observed,[81,82] yet obtaining single crystals of sufficient size and quality suitable for diffraction analysis proves elusive. In this context, it is to be remembered that NMR is a probe of the local chemical environment around a nucleus. As such, high-resolution MAS NMR spectra can be expected for a powdered sample comprising individual crystals that are considerably smaller than are required to obtain a single-crystal diffraction structure.

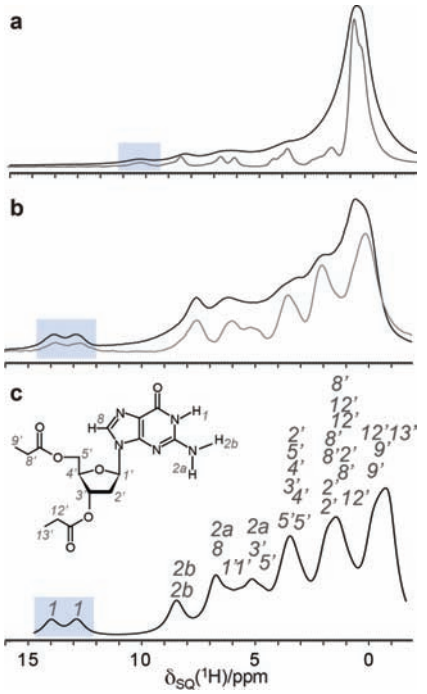

Figure 3. ^{1}H NMR spectra of (a) **1** and (b and c) **2**. (a and b) ^{1}H (600 MHz) fast MAS (30 kHz, black) and homonuclear (DUMBO) decoupled (12.5 kHz MAS, gray) NMR spectra. The highlighted spectral regions correspond to the hydrogen-bonded NH resonances. (c) Computed GIPAW ^{1}H chemical shifts as determined for the geometrically optimized (CASTEP) crystal structure, convoluted with 500 Hz Lorentzian line broadening and with site assignments shown.

Notably, the observation of only one resonance per chemically distinct carbon atom in the ^{13}C CP MAS spectrum in Figure 2a suggests that **1** adopts a distinctly different solid-state structure as compared to **2**, as previously demonstrated by ^{15}N refocused INADEQUATE spectra of ^{15}N-labeled **1** and **2**.[68] Indeed, the question then arises can the observation of one or two resonances per chemically distinct carbon atom be interpreted as being directly indicative of quartet-like or ribbon-like self-assembly?

^{1}H Solid-State NMR of dG(C10)$_2$ (1) and dG(C3)$_2$ (2). In ^{1}H solid-state NMR, MAS does not completely remove the line broadening due to homonuclear ^{1}H−^{1}H dipolar couplings, with the resolution improving as the MAS frequency increases.[83] Enhanced resolution can be achieved by combining physical spinning under MAS with carefully synchronized rotations of the spins using *rf* pulses in the so-called CRAMPS (combined rotation and multiple-pulse spectroscopy) approach.[84−87] Figure 3a and 3b presents ^{1}H solid-state NMR spectra of **1** and **2**; it is evident that enhanced resolution is achieved using CRAMPS at a moderate MAS frequency (12.5 kHz MAS with DUMBO decoupling, gray) as compared to fast MAS (30 kHz, black).

Fast MAS alone is sufficient to resolve the high-ppm hydrogen-bonding resonances that are indicated by blue shading in Figure 3a and 3b. For **2** (Figure 3b), a clear doubling of peaks is evident, due to the presence of two distinct molecules in the asymmetric unit for the ribbon architecture. These resonances are also shifted downfield (to high ppm) by roughly 3−4 ppm with respect to the highest ^{1}H resonance of **1** (Figure 3a), indicating a distinctly different hydrogen-bonding arrangement between the two compounds. Figure 3c presents a simulated spectrum based on the GIPAW-computed ^{1}H chemical shifts of **2**, with an applied line broadening of 500 Hz; good agreement with the ^{1}H DUMBO spectrum in Figure 3b is observed.

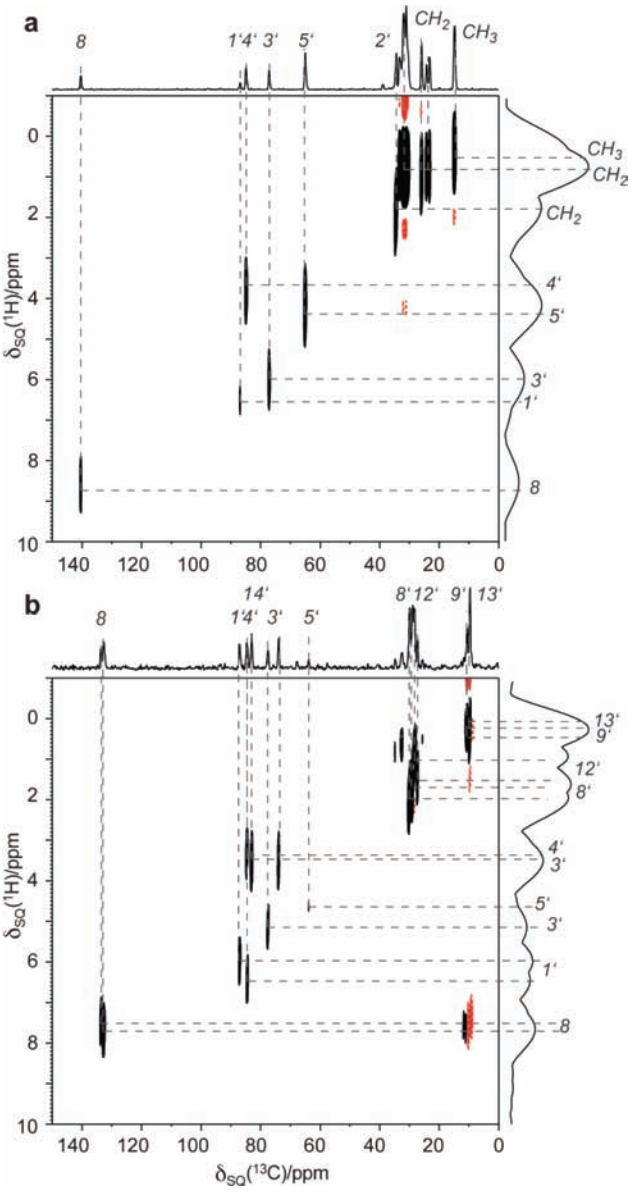

Figure 4. ^{1}H (600 MHz, DUMBO)−^{13}C refocused INEPT spectra of (a) **1** and (b) **2**, recorded at 12.5 kHz MAS, together with skyline projections. Assignments of ^{13}C and ^{1}H chemical shifts are based on (GIPAW) calculated shieldings determined for **2**, as given in Figures 2c and 3c. The base contour level is at (a) 9% and (b) 15% of the maximum peak height in each spectrum, and negative contours are shown in red. (b) The apparent peak with positive and negative intensity at a ^{1}H chemical shift of ∼8 ppm for the 9′ and 13′ ^{13}C resonances is an artifact of the ^{1}H homonuclear decoupling.

^{1}H−^{13}C SQ-SQ Refocused INEPT 2D NMR Spectra of dG(C10)$_2$ (1) and dG(C3)$_2$ (2). Figure 4a and 4b presents ^{1}H−^{13}C heteronuclear correlation spectra of **1** and **2**, respectively, recorded at 12.5 kHz MAS using the refocused INEPT[88] pulse sequence with eDUMBO$_{22}$ homonuclear decoupling[89] applied to achieve high resolution in the indirect ^{1}H dimension. Short (<1.5 ms) $\tau = \tau'$ periods (with eDUMBO$_{22}$ homonuclear decoupling[89]) were used for the refocused INEPT transfer, such that correlation peaks are observed only for directly bonded pairs of ^{13}C−^{1}H nuclei.

Table 1. ^{13}C and ^{1}H Chemical Shifts of 1 and 2

site	mol	$\delta(^{13}C/^{1}H)$/ppm[a,b] expt 1	$\delta(^{13}C/^{1}H)$/ppm[a,b] expt 2	$\delta(^{13}C/^{1}H)$/ppm[c] calcd 2
C11′	A	174.3	176.6	178.8
	B		177.1	180.8
C7′	A	172.6	174.9	171.1
	B		175.4	177.9
C6	A	158.5	159.0	156.8
	B		159.0	156.7
C2 [d]	A	153.6	154.6	150.4
	B		154.6	151.0
C4 [d]	A	152.4	150.2	150.0
	B		151.9	151.6
CH8	A	140.4	132.9	130.3
	B		134.3	132.4
CH5	A	117.8	116.2	117.5
	B		115.3	117.1
CH1′	A	86.7	87.0	88.9
	B		84.5	86.1
CH4′	A	84.9	84.5	86.1
	B		83.1	84.8
CH3′	A	77.0	77.5	78.2
	B		73.9	74.3
CH5′	A	64.9	63.7	62.6
	B		63.7	62.9
CH2′	A	39.0	42.7	38.8
	B		40.2	35.5
CH12′	A	23.2−34.6[e]	27.1	25.4
	B		28.2	27.3
CH8′	A		28.8	22.8
	B		29.9	25.1
CH9′	A	15.0	10.3	4.7
	B			6.3
CH13′	A	14.6	9.4	2.1
	B			5.8
NH1	A	10.5	13.2	13.0
	B		14.0	14.1
NH2a	A	8.5	5.6	5.3
	B		6.1	6.9
NH2b	A	6.8	7.5	8.6
	B		8.0	8.5
CH8	A	8.7	7.7	6.8
	B		7.5	6.9
CH1′	A	6.6	6.0	5.8
	B		6.2	6.3
CH4′	A	3.6	3.5	3.5
	B		3.3	3.3
CH3′	A	6.0	5.2	5.2
	B		3.5	3.7
CH5′a	A	4.3	4.8	4.8
	B		3.5	3.7
CH5′b	A		3.0	3.0
	B		3.7	4.0
CH2′a	A	4.0	2.2	2.1
	B		1.4	1.4
CH2′b	A	2.2	2.2	2.0
	B		3.5	3.5
CH12′a	A	2.5[e]	1.5	1.5
	B		1.0	0.0
CH12′b	A	1.8[e]	1.5	1.4
	B		1.0	0.9
CH8′a	A	0.8[e]	2.0	1.8
	B		1.7	1.5
CH8′b	A	0.8[e]	2.0	1.2
	B		2.0	1.9
CH9′	A	0.5	0.5	−0.1[f]
	B		0.2	−0.4[f]
CH13′	A	0.5	0.0	−0.8[f]
	B		0.0	−0.8[f]

[a] As determined from ^{13}C CP MAS (Figure 2) and ^{1}H (DUMBO)−^{13}C refocused INEPT (Figure 4) spectra. [b] As determined from ^{1}H MAS (Figure 3), ^{1}H (DUMBO)−^{13}C refocused INEPT (Figure 4), and ^{1}H DQ-SQ CRAMPS (DUMBO, Figures 5 and 6) spectra. [c] Calculated (GIPAW) chemical shifts using $\sigma_{ref}(^{13}C)$ = 168.1 ppm and $\sigma_{ref}(^{1}H)$ = 29.97 ppm, as determined by a procedure that ensured that the mean of the calculated and experimental chemical shifts for all sites in **2** coincide. [d] Tentative assignment of experimental ^{13}C chemical shifts for nonprotonated carbon resonances. [e] Range of alkyl CH_2 resonances (cf. CH8′, CH12′ for **2**) observed for **1**, with ^{13}C chemical shifts not individually assigned. ^{1}H chemical shifts identified based on $^{1}H-^{1}H$ proximities observed in Figure 6c and Table S6, Supporting Information, but not necessarily assigned to sites shown. [f] Average of the calculated ^{1}H chemical shifts for the CH_3 protons CH9′ and CH13′.

The through-bond transfer of ^{1}H magnetization to the well-resolved ^{13}C nuclei allows the ^{1}H chemical shifts of protons directly bonded to carbons to be assigned for **1** and **2**, as tabulated in Table 1. Note that no correlation peaks are observed for ^{1}H nuclei that are not directly bonded to ^{13}C nuclei, i.e., the $^{1}H-^{13}C$ refocused INEPT experiment does not provide insight into the ^{1}H chemical shifts of the NH and NH_2 protons. The NH and NH_2 ^{1}H chemical shifts can be determined, however, from the ^{1}H DQ spectra presented below, as well as $^{1}H-^{15}N$ and $^{1}H-^{14}N$ correlation spectra that are also presented below for **2**. In addition, correlation peaks are weak or not visible at the contour level shown in Figure 4b for the ^{1}H resonances of the CH_2 groups in the sugar ring, CH2′ and CH5′. As noted in refs 80, 90, and 91, this is due to the faster dephasing of ^{1}H and ^{13}C magnetization for a CH_2 group as compared to a CH group. Correlations resulting from the alkyl CH_2 resonances (CH8′ and CH12′ in Figure 4b), however, are observed for these compounds. It should be noted that while the CH_2 and CH_3 resonances (CH8′, CH9′, CH12′, and CH13′) can be separately identified (and chemical shifts assigned by comparison to computed values) for **2**, the multiple sites of the long alkyl chains in **1** result in many ^{1}H and ^{13}C resonances between $\delta_{SQ}(^{13}C)$ = 20 and 35 ppm in Figure 4a. No attempt is made here to distinguish each of the ^{13}C chemical shifts in this region, and as such they are collectively referred to as the CH_2 and CH_3 resonances of the alkyl chain in Figure 4a.

$^{1}H-^{1}H$ DQ-SQ 2D NMR Spectra of dG(C10)$_2$ (1) and dG-(C3)$_2$ (2). Figures 5 and 6 present high-resolution ^{1}H DQ-SQ correlation spectra of **2** and **1**, respectively, recorded under fast (30 kHz) MAS alone (Figures 5a and 6a) and DUMBO homonuclear decoupling (CRAMPS) at a MAS frequency of 12.5 kHz (Figures 5b−d and 6b−d).

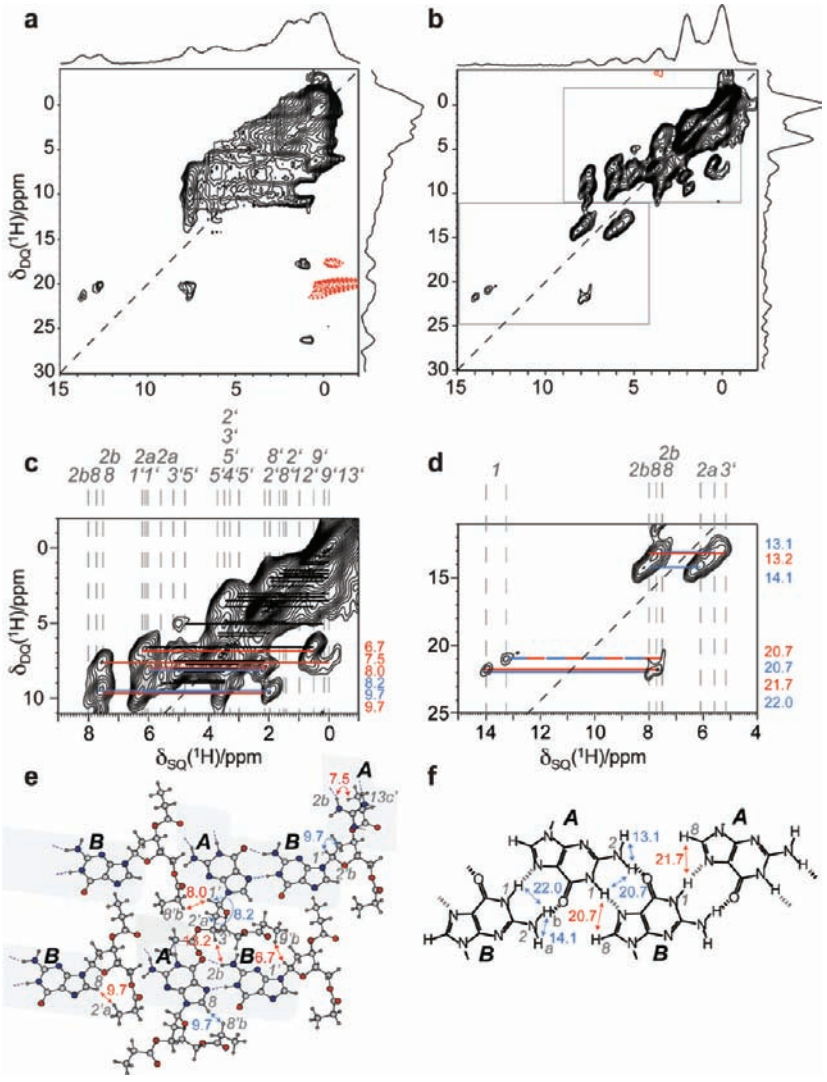

Figure 5. ^{1}H (600 MHz) DQ NMR spectra together with skyline projections of **2**: (a) ^{1}H−^{1}H DQ-SQ MAS spectrum recorded at 30 kHz MAS, (b) ^{1}H−^{1}H DQ (DUMBO)-SQ (DUMBO) CRAMPS spectrum recorded at 12.5 kHz MAS. One rotor period of BABA recoupling or three POST-C7 elements were used for excitation and reconversion of DQ coherence in a and b, respectively. The base contour level is at (a) 2% or (b−d) 3% of the maximum peak height in each spectrum, and negative contours are shown in red. In all spectra, the $F_1 = 2F_2$ diagonal is shown as a black dashed line. The regions within the rectangles in b correspond to the expanded regions in c and d, where site assignments are shown and DQ correlations are indicated by solid horizontal bars. Blue and red bars in c and d highlight DQ coherences arising from pairs of intra- and intermolecular ^{1}H−^{1}H nuclei, respectively, as discussed in the text. (e and f) Representations of the ribbon-like structure of **2** showing the H−H proximities corresponding to the assigned DQ peaks in (c and d). The H−H proximities are labeled with their ^{1}H DQ chemical shift (see Tables 2 and S3 and S4, Supporting Information).

As in previous applications of the ^{1}H DQ CRAMPS experiment,[91−101] it is clear that the resolution is much superior as compared to the fast-MAS DQ experiment.[84,102,103] The expanded regions in Figures 5c, 5d, 6c, and 6d show the ^{1}H DQ-SQ CRAMPS correlation peaks in more detail for the highlighted spectral regions in Figures 5b and 6b. Table 2, along with Tables S3 and S4 in the Supporting Information, list the ^{1}H DQ peaks that are expected on the basis of the H−H proximities identified in the (CASTEP-optimized) single-crystal diffraction structure of **2** for the assigned chemical shifts in Table 1, specifically, ^{1}H DQ correlations in Figure 5 involving NH, NH_2, and CH8 ^{1}H nuclei (Table 2), among alkyl ^{1}H nuclei (Table S3, Supporting Information) and involving sugar ^{1}H nuclei (Table S4, Supporting Information). For **1**, for which there is no single-crystal diffraction structure, Table S6 in the Supporting Information lists the resolved ^{1}H DQ correlations observed in Figure 6.

As shown in the expanded regions in Figure 5c and 6c, the enhanced resolution provided by the ^{1}H DQ-SQ CRAMPS experiment is particularly evident for the crowded regions corresponding to $\delta_{SQ}(^1H) < 7$ ppm. Consider first the crowded low-ppm $\delta_{DQ}(^1H) <$ 5 ppm region corresponding to the DQ coherences between and among the alkyl chain groups, as listed in Table S3, Supporting Information, for **2** and Table S6, Supporting Information, for **1**. For **2**, peaks corresponding to DQ coherences are expected for the H−H proximities (1.75−1.78 Å) within the CH_3 groups at $\delta_{DQ} = 0.0 + 0.0 = 0.0$ ppm (CH13′A, B), 0.2 + 0.2 = 0.4 ppm (CH9′B), and 0.5 + 0.5 = 1.0 ppm (CH9′A) and the CH_2 groups at δ_{DQ} = 1.0 +1.0 = 2.0 ppm (CH12′B), 1.5 + 1.5 = 3.0 ppm (CH12′A), 2.0 + 1.7 = 3.7 ppm (CH8′B), and 2.0 + 2.0 = 4.0 ppm (CH8′A). In addition, Table S3, Supporting Information, lists various intramolecular proximities between the distinct CH_3 and CH_2 groups in the distance range 2−3 Å corresponding to δ_{DQ} between 0 and 3.5 ppm.

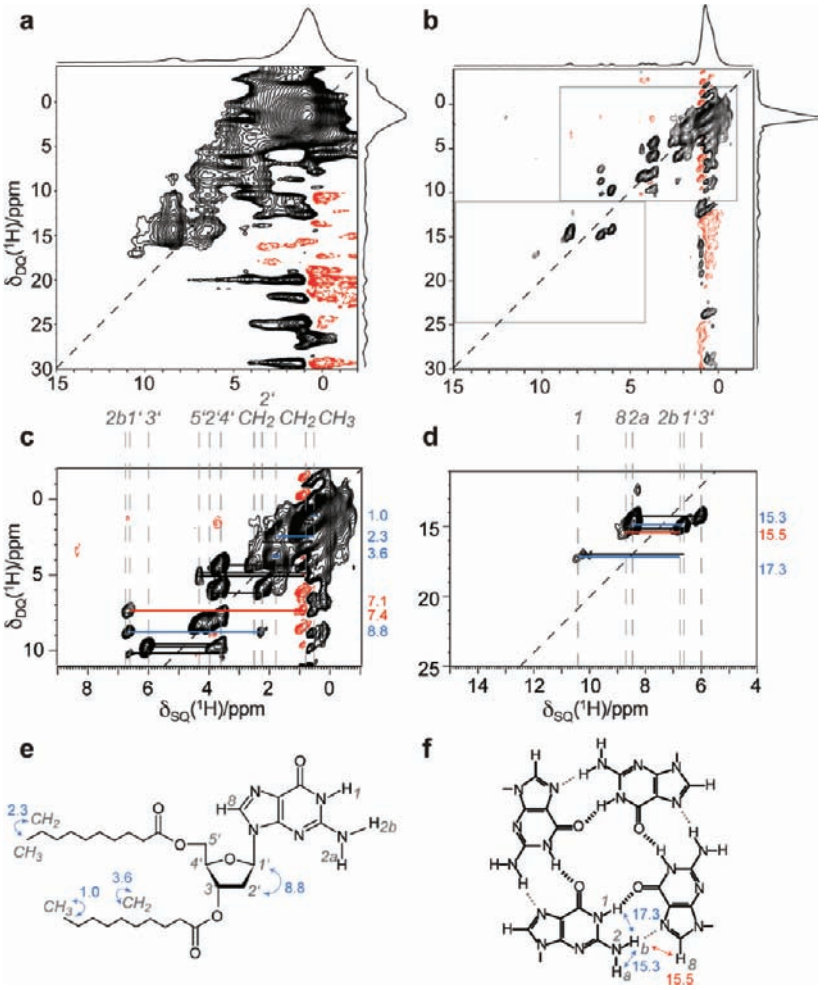

Figure 6. ^{1}H (600 MHz) DQ NMR spectra together with skyline projections of **1**: (a) ^{1}H−^{1}H DQ-SQ MAS spectrum recorded at 30 kHz MAS, (b) ^{1}H−^{1}H DQ (DUMBO)-SQ (DUMBO) CRAMPS spectrum recorded at 12.5 kHz MAS. One rotor period of BABA recoupling or three POST-C7 elements were used for excitation and reconversion of DQ coherence in a and b, respectively. The base contour level is at (a) 3% or (b−d) 1% of the maximum peak height in each spectrum, and negative contours are shown in red. In all spectra, the $F_1 = 2F_2$ diagonal is shown as a black dashed line. The regions within the rectangles in b correspond to the expanded regions in c and d, where site assignments are shown and DQ correlations are indicated by solid horizontal bars. Blue and red bars in c and d highlight DQ coherences arising from pairs of intra- and intermolecular ^{1}H−^{1}H nuclei, respectively, as discussed in the text. (e and f) Molecular structure and representations of the quartet-like structure of **1** showing the H−H proximities corresponding to the assigned DQ peaks in c and d, and the H−H proximities are labeled with their ^{1}H DQ chemical shift (see Table S6, Supporting Information).

The expanded regions in Figures 5c and 6c also contain DQ correlations involving ^{1}H nuclei of the sugar ring (listed in Tables S4 and S6, Supporting Information, for **2** and **1**, respectively). Prominent pairs of peaks are observed in both spectra arising from the same intramolecular H1′−H2′ proximities (**2**: δ_{DQ} = 6.0 + 2.2 = 8.2 ppm (CH1′A- CH2′aA, 2.44 Å); δ_{DQ} = 6.2 + 3.5 = 9.7 ppm (CH1′B −CH2′bB, 2.44 Å); **1**: δ_{DQ} = 6.6 + 2.2 = 8.8 ppm). The intramolecular proximities evident from Figures 5c and 6c are indicated in blue in Figures 5e and 6e, where they are labeled with the corresponding ^{1}H DQ chemical shifts. Interestingly, Figure 5c (for **2**) also shows pairs of peaks assigned to DQ coherences due to *intermolecular* proximities (shown in red) between a sugar ^{1}H nucleus and an alkyl proton of a neighboring molecule: δ_{DQ} = 6.2 + 0.5 = 6.7 ppm (CH1′B−CH9′bA, 2.24 Å); δ_{DQ} = 6.0 + 2.0 = 8.0 ppm (CH1′A−CH8′bB, 2.49 Å). The representation of the optimized crystal structure of **2** in Figure 5e (see middle region) shows that these proximities between the two distinct molecules arise due to the vertical stacking of the planar ribbon structures. It is to be noted that DQ correlations corresponding to proximities between a sugar ^{1}H nucleus and alkyl protons are also observed for **1**: H1′−CH_3 or CH_2 δ_{DQ} = 6.6 + 0.5 = 7.1 ppm and 6.6 + 0.8 = 7.4 ppm (see Table S6, Supporting Information); these are highlighted by red horizontal bars in Figure 6c. DQ correlation peaks due to H−H proximities involving the NH protons are identified in the expanded regions given in Figures 5d and 6d and tabulated in Table 2 for **2** or Table S6, Supporting Information, for **1**. The internal geometry of the NH (NH1) and NH_2 (NH2a,b) protons of the guanine headgroup gives rise to close intramolecular proximities that enable assignment of the ^{1}H NH_2 chemical shifts: for **2** δ_{DQ} = 13.2 + 7.5 = 20.7 ppm (NH1A−NH2bA, 2.36 Å), δ_{DQ} = 14.0 + 8.0 = 22.0 ppm (NH1B−NH2bB, 2.34 Å), δ_{DQ} = 5.6 + 7.5 = 13.1 ppm (NH2aA−NH2bA, 1.75 Å), δ_{DQ} = 6.1 + 8.0 = 14.1 ppm (NH2aB−NH2bB, 1.75 Å); for **1** δ_{DQ} = 10.5 + 6.8 = 17.3 ppm (NH1−NH2b); δ_{DQ} = 6.8 + 8.5 = 15.3 ppm (NH2b−NH2a). Rows extracted at these ^{1}H DQ frequencies from the ^{1}H−^{1}H DQ (DUMBO)-SQ (DUMBO) CRAMPS spectra (see Figures 5d and 6d) are shown in Figure S4 in the Supporting

Table 2. ^{1}H DQ Correlations[a] Involving NH, NH_2, and CH8 ^{1}H Nuclei (<3.0 Å) in **2** (see Figure 5d)

proton	δ_{SQ} (^{1}H)/ppm	proton	δ_{SQ} (^{1}H)/ppm	separation[b]/Å	δ_{DQ} (^{1}H)/ppm
CH8′a B	**1.7**	**NH2a A**	**5.6**	**2.96**	**7.3**
CH13′c B	**0.0**	**NH2b A**	**7.5**	**2.97**	**7.5**
CH8′b B	2.0	NH2a B	6.1	2.83	8.1
CH4′B	**3.3**	**NH2a A**	**5.6**	**2.85**	**8.9**
CH2′a B	1.4	CH8 B	7.5	2.92	8.9
CH2′b B	**3.5**	**NH2a A**	**5.6**	**2.56**	**9.1**
CH5′a B	**3.5**	**NH2a A**	**5.6**	**2.84**	**9.1**
CH12′a A	**1.5**	**NH2b B**	**8.0**	**2.71**	**9.5**
CH8′b A	2.0	CH8 A	7.7	2.52	9.7
CH2′a A	**2.2**	**CH8 B**	**7.5**	**2.53**	**9.7**
NH2a A	5.6	NH2b A	7.5	1.75	13.1
CH3′A	**5.2**	**NH2b B**	**8.0**	**2.70**	**13.2**
CH13′b B	**0.0**	**NH1 A**	**13.2**	**2.83**	**13.2**
CH13′b A	**0.0**	**NH1 B**	**14.0**	**2.88**	**14.0**
NH2a B	6.1	NH2b B	8.0	1.75	14.1
CH12′b A	1.5	NH1 A	13.2	2.90	14.7
CH12′b B	1.0	NH1 B	14.0	2.90	15.0
CH8 B	**7.5**	**NH1 A**	**13.2**	**2.88**	**20.7**
NH2b A	7.5	NH1 A	13.2	2.36	20.7
CH8 A	**7.7**	**NH1 B**	**14.0**	**2.84**	**21.7**
NH2b B	8.0	NH1 B	14.0	2.34	22.0

[a] Intermolecular proximities are given in bold typeface. [b] H−H distances from the (CASTEP) geometrically optimized crystal structure.

Information. For **1**, so-called t_1 noise due to dynamics in the long alkyl chains is evident as strong positive and negative intensity at the alkyl chain SQ frequency (~1 ppm) in the ^{1}H DQ spectra in Figure 6. This has been observed in ^{1}H DQ spectra of other organic molecules with long alkyl chains;[84] as shown in the extracted rows in Figure S4, Supporting Information, this does not obscure other DQ peaks. It is evident that as well as the significantly different ^{1}H NH chemical shifts for **1** and **2** noted above, the relative magnitude of the NH_2, NH2a, and NH2b chemical shifts is also interchanged, i.e., the NH_2 proton closest to the NH proton has the bigger ^{1}H chemical shift for **2** but the smaller ^{1}H chemical shift for **1**. For **2**, from the crystal structure,[33] the second NH_2 hydrogen atom (NH2a) that does not participate in the ribbon-like hydrogen bonding forms intermolecular NH···O hydrogen bonds with the side chain carbonyl oxygen atoms. These NH···O hydrogen-bond lengths are longer (3.14 and 2.93 Å compared to 2.86 and 2.86 Å for the intraribbon NH···O hydrogen bond in Figure 1b) and deviate further from linearity (134° and 157° compared to 159°and 157°), and this is reflected in the smaller ^{1}H chemical shifts. For **1**, there is no single-crystal diffraction structure; however a quartet-like self-assembly has been identified by means of ^{15}N refocused INADEQUATE solid-state NMR spectra.[68] The different relative magnitude of the NH_2 ^{1}H hemical shifts indicates that the second NH_2 hydrogen atom (NH2a) that does not participate in the quartet-like hydrogen bonding does, however, participate in a strong hydrogen-bonding interaction with a donor atom external to the quartet-like arrangement. In this context, Ciesielski et al. proposed that formation of N2···N3 hydrogen bonds between adjacent guanosine quartets explains the close packing of guanosine quartets on a surface, as observed by STM.[104]

Table 1 shows that the chemical shift of the guanine CH8 aromatic proton is similar to that of an NH_2 proton in both **1** and **2** (noting that the CH8 ^{1}H chemical shifts can be accurately determined from the ^{1}H−^{13}C heteronuclear correlation spectra in Figure 4). For **2**, as listed in Table 2, there are intermolecular, intraribbon H−H proximities for CH8−NH1 (see Figure 5f) with distances of 2.88 and 2.84 Å. While the corresponding DQ peaks at δ_{DQ} = 7.5 + 13.2 = 20.7 ppm and δ_{DQ} = 7.7 + 14.0 = 21.7 ppm overlap with those due to the NH−NH_2 proximities noted above (at 20.7 and 22.0 ppm), for the DQ peaks at δ_{DQ} = 22.0 and 21.7 ppm there appear to be two separate peaks at δ_{SQ} = 8.0 ppm (NH2bB) and δ_{SQ} = 7.7 ppm (CH8A) in Figure 5d. In addition, for **2**, there are H−H proximities between the guanine CH8 aromatic protons and the aliphatic protons that give rise to evident DQ peaks in Figure 5c at δ_{DQ} = 7.7 + 2.0 = 9.7 ppm (CH8A−CH8′bA, 2.52 Å) and δ_{DQ} = 7.5 + 2.2 = 9.7 ppm (CH8B−CH2′aA, 2.53 Å), while the DQ peaks at δ_{DQ} = 7.5 + 0.0 = 7.5 ppm (NH2bA−CH13′cB, 2.97 Å) are due to intermolecular H−H proximities between NH2bA and methyl-group protons (see top right-hand corner of Figure 5e).

For **1**, the CH8 ^{1}H chemical shift of 8.7 ppm is also very similar to that of the NH_2 (NH2a) proton at 8.5 ppm. As for **2**, DQ peaks can be expected for a CH8−NH2b proximity (see Figure 6d and 6f) at δ_{DQ} = 8.7 + 6.8 = 15.5 ppm, with these DQ peaks overlapping with those due to the NH2a−NH2b proximity at δ_{DQ} = 8.5 + 6.8 = 15.3 ppm. In addition, there is a clear pair of DQ peaks at δ_{DQ} = 8.7 + 6.0 = 14.7 ppm in Figure 6d. From this spectrum, however, it cannot be established categorically if this indicates a H−H proximity between the CH3′ proton at 6.0 ppm and the CH8 proton at 8.7 ppm or alternatively with the NH_2 (NH2a) proton at 8.5 ppm. For **2**, it is to be noted that Table 2 indicates that there is a 2.70 Å intermolecular proximity between a pair of NH_2 (NH2b) and CH3′ protons that would also give rise to DQ peaks at δ_{DQ} = 8.0 + 5.2 = 13.2 ppm.

^{1}H (DQ-DUMBO)−^{13}C SQ Refocused INEPT 2D NMR Spectrum of dG(C3)$_2$ (2). Clear identification of distinct DQ peaks

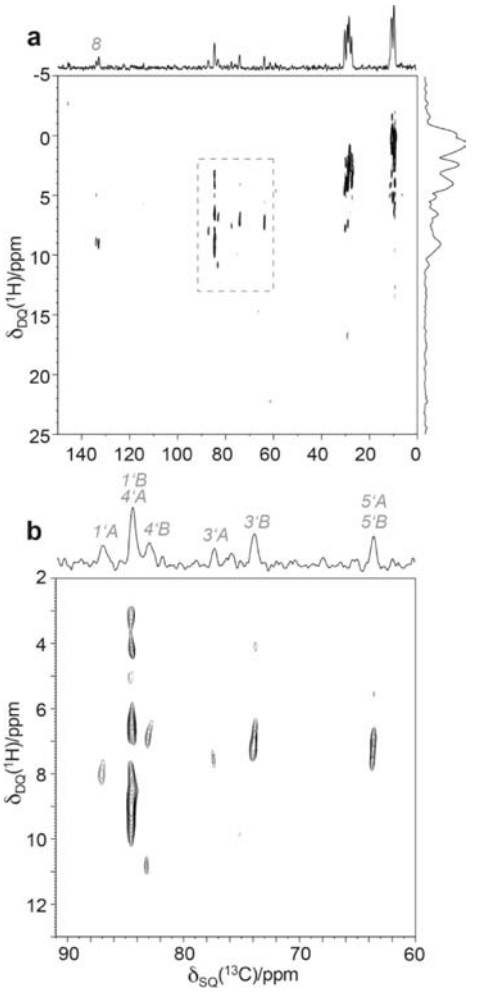

Figure 7. ^{1}H (600 MHz) (DQ-DUMBO)−^{13}C refocused INEPT spectrum of **2**, recorded at 12.5 kHz MAS, together with skyline projections. (b) Expanded region corresponding to the sugar ^{13}C resonances; see Table S7, Supporting Information, for a listing of expected ^{1}H DQ peaks. Three POST-C7 elements were used for excitation and reconversion of DQ coherence. Base contour level is at 16% of the maximum peak height in each spectrum, and negative contours are shown in red.

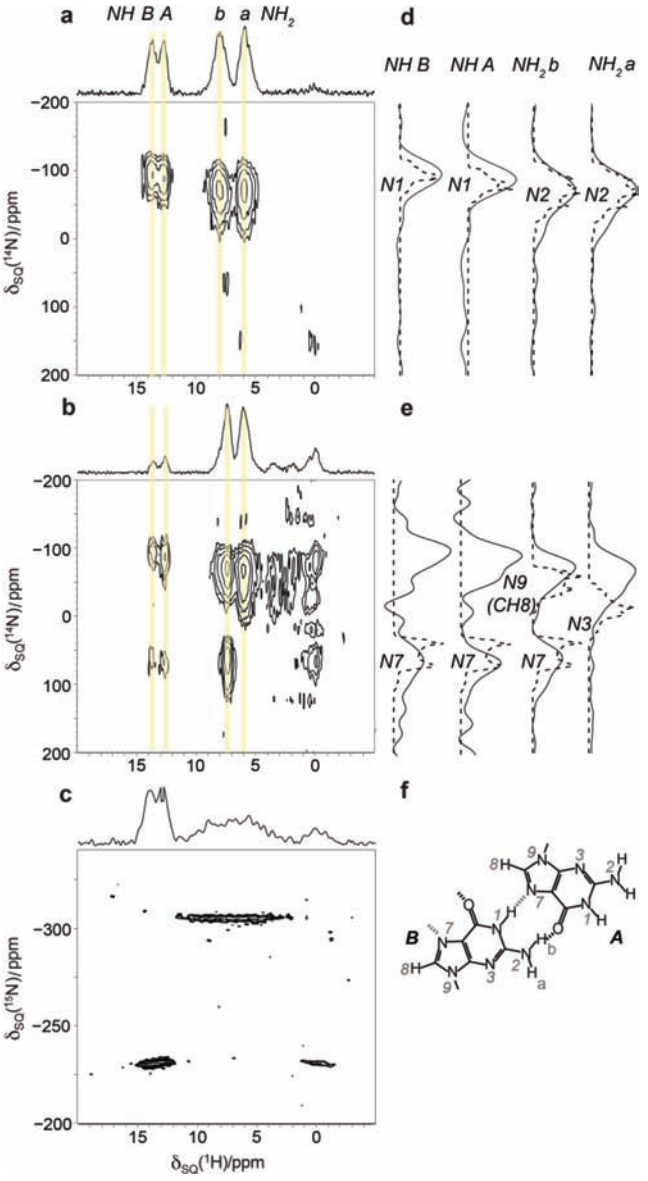

Figure 8. (a and b) ^{14}N−^{1}H (850 MHz, 60 kHz MAS) HMQC spectra of **2** recorded using n = 2 rotary resonance recoupling (R^3) of the ^{14}N−^{1}H heteronuclear dipolar couplings with duration (a) 167 and (b) 667 μs. (c) ^{1}H−^{15}N (600 MHz, 22 kHz MAS) REPT-HSQC spectrum of ^{15}N-labeled **2** recorded using one rotor period of REDOR recoupling of the ^{1}H−^{15}N heteronuclear dipolar couplings. Skyline projections are shown for the ^{1}H dimension. Base contour level is at (a) 14%, (b) 8%, and (c) 15%. (d and e) Comparison of experimental ^{14}N spectra (solid lines) corresponding to columns through the NH or NH_2 ^{1}H resonances, with spectra simulated (dashed lines) using SPINEVOLUTION[110] for the previously determined experimental isotropic ^{15}N (same as ^{14}N) chemical shifts[71] and quadrupolar parameters as calculated using the GIPAW method. (C_Q values have been scaled by a consistent factor of 0.96 to give best alignment of simulated and experimental ^{14}N line shapes; see Table S2, Supporting Information, for calculated quadrupolar parameters.) (f) Schematic representation of intermolecular hydrogen bonding in **2**.

due to the CH8 aromatic protons is possible by means of the ^{1}H (DQ-DUMBO)−^{13}C SQ refocused INEPT experiment.[91] As shown in Figure 7a, such a ^{1}H DQ−^{13}C SQ spectrum for **2** correlates the ^{13}C resonance of a specific protonated carbon atom with ^{1}H DQ coherences due to H−H proximities involving the proton(s) that are directly bonded to that carbon atom. The better resolution of distinct ^{1}H DQ peaks in a ^{1}H DQ−^{13}C SQ spectrum as compared to in a ^{1}H−^{1}H DQ-SQ spectrum comes at the expense of much reduced sensitivity: the spectrum in Figure 7 required 80 h of experimental time on a 850 MHz spectrometer, as compared to 1 h only at 600 MHz for the ^{1}H−^{1}H DQ-SQ CRAMPS spectra in Figures 5 and 6. The ^{1}H DQ−^{13}C SQ spectrum in Figure 7 was recorded with the same DQ recoupling time (three POST-C7 elements) as for the ^{1}H−^{1}H DQ-SQ CRAMPS spectra. For the CH8 resonances at 132.9 and 134.3 ppm, ^{1}H DQ peaks are only observed for the closest H−H proximities at δ_{DQ} = 7.7 + 2.0 = 9.7 ppm (CH8A−CH8′bA, 2.52 Å) and δ_{DQ} = 7.5 + 2.2 = 9.7 ppm (CH8B−CH2′aA, 2.53 Å) corresponding to the proximities to alkyl chain and sugar ring CH_2 protons noted above and identified in Figure 5e. As shown in the expanded region in Figure 7b, the ^{1}H DQ−^{13}C SQ experiment also allows a clear resolution and identification of distinct ^{1}H DQ peaks involving the sugar protons. Table S7, Supporting Information, lists the expected positions of peaks for the sugar

dx.doi.org/10.1021/ja206516u |J. Am. Chem. Soc. 2011, 133, 19777–19795

^{13}C resonances corresponding to the expanded spectral region in Figure 7b.

^{1}H−^{15}N and ^{14}N−^{1}H 2D NMR Spectra of dG(C3)$_2$ (2). The ^{1}H chemical shifts for NH and NH$_2$ groups can be unambiguously assigned by means of nitrogen−proton correlation experiments. In particular, it has recently been shown that ^{14}N−^{1}H correlation spectra[105] can be recorded for the spin I = 1 ^{14}N nucleus (99.6% natural abundance) using either the small J and residual second-order quadrupolar-dipolar couplings[106] or the larger heteronuclear dipolar couplings for coherence transfer.[107] ^{14}N−^{1}H correlation experiments benefit from high magnetic field so as to reduce the anisotropic second-order quadrupolar broadening in the ^{14}N dimension as well as fast MAS to reduce the ^{1}H dipolar-broadened line shapes and to extend the ^{1}H coherence lifetimes.[108] This is demonstrated in Figure 8 for **2**, whereby Figure 8a and 8b present ^{14}N−^{1}H HMQC (heteronuclear multiple-quantum correlation) spectra recorded at 850 MHz and 60 kHz MAS using n = 2 rotary resonance recoupling (R^3)[109] of the ^{14}N−^{1}H heteronuclear dipolar couplings.

Different R^3 durations of (a) 167 and (b) 667 μs were used to record the spectra presented in Figure 8a and 8b. For the shorter recoupling time, only one-bond N−H correlations are observed. Considering the four peaks observed in Figure 8a, the peaks at ^{1}H chemical shifts of 13 and 14 ppm correspond to the two crystallographically distinct NH sites. For the NH$_2$ moieties, there should be four distinct peaks; however, the ^{1}H chemical shifts of the two NH2a sites (5.6 and 6.1 ppm) and the two NH2b sites (7.5 and 8.0 ppm) are not resolved, and both separate peaks correspond to a superposition of ^{14}N line shapes for the two distinct NH$_2$ groups. Figure 8d presents experimental columns (solid lines) through the two distinct NH resonances and the two distinct NH$_2$ resonances together with spectra simulated (dashed lines) using the previously determined experimental isotropic ^{15}N (same as ^{14}N) chemical shifts[71] and quadrupolar parameters as calculated using the GIPAW method (see Table S2, Supporting Information). Note that the calculated C_Q values have been scaled by a consistent factor of 0.96 to ensure best alignment of simulated and experimental ^{14}N line shapes.

In Figure 8b, longer range N−H correlations are also observed. As well as additional peaks due to through-space proximities of the sugar and alkyl protons to the NH and NH$_2$ nitrogen atoms, of particular interest are the evident additional peaks at a ^{14}N shift of ∼60 ppm. Considering the strongest peak at the NH2b ^{1}H chemical shift of ∼8 ppm, this is assigned to a through-space proximity to the N7 nitrogen on the opposite hydrogen-bonding face (see Figure 8f); Figure 8e compares the experimental ^{14}N line shape with that simulated using the experimental ^{15}N isotropic chemical shift and the calculated (GIPAW) quadrupolar parameters for N7. It is to be noted that the CH8 ^{1}H chemical shifts (7.5 and 7.7 ppm) overlap with those for the NH2b protons, and intramolecular proximities are expected for the N7 and N9 nitrogen atoms. (Table S8, Supporting Information, lists the distances between the NH, NH$_2$, and CH8 hydrogen atoms and the nitrogen atoms, as extracted from the geometrically optimized crystal structure.) It is striking that there is no peak at ∼60 ppm for the NH2a ^{1}H chemical shift of ∼6 ppm, since the NH2a proton is pointing away from the N7 nitrogen atom. Weaker peaks are observed at a ^{14}N shift of ∼60 ppm for the NH ^{1}H chemical shifts which correspond to the N1−H···N7 hydrogen bonds; in this respect, note that the one-bond correlation peaks for the NH groups are also of considerably weaker intensity than those for

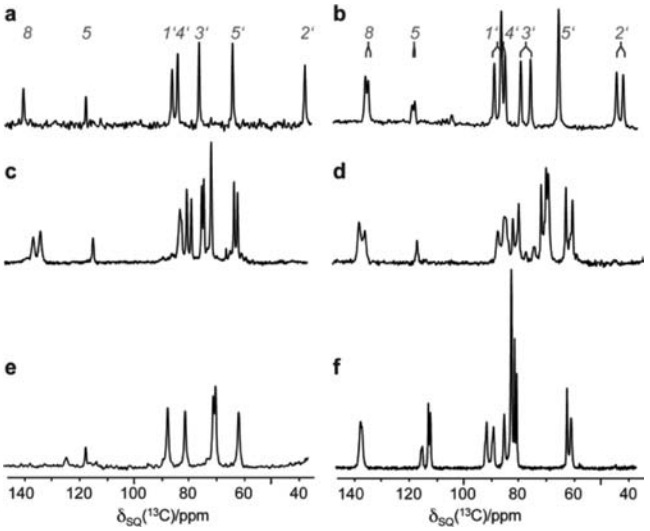

Figure 9. ^{13}C CP MAS spectra of (a) **1**, (b) **2**, (c) **3**, (d) **4**, (e) **5**, and (f) **6**, expanded to show the ^{13}C resonances around the sugar and guanine CH5 and CH8 region. Spectra were recorded at Larmor and MAS frequencies of (a) 150 MHz and 8 kHz, (b and e) 150 MHz and 12.5 kHz, and (c, d, and f) 75 MHz and 8.5 kHz. Site assignments for 1 and 2 are from Table 1.

the NH$_2$ groups, with this indicating a faster dephasing of the NH magnetization during the longer R^3 recoupling period. The NH2a protons have an intramolecular proximity to the N3 nitrogen atoms; this results in a shoulder at ∼0 ppm, as shown in the NH2a column in Figure 8e, where the dashed line is the simulated spectrum for the N3 nitrogen.

For comparison, Figure 8c presents a ^{1}H−^{15}N REPT-HSQC (recoupled polarization transfer heteronuclear single-quantum correlation)[111] correlation spectrum recorded at 600 MHz and 22 kHz MAS for a ^{15}N-labeled sample of **2**, for which ^{15}N refocused INADEQUATE and spin−echo results have been presented in refs 68 and 71. The spectrum has been rotated through 90° (in the ^{1}H−^{15}N REPT-HSQC experiment, the F_1 and F_2 dimensions correspond to ^{1}H and ^{15}N, respectively, as compared to ^{14}N and ^{1}H in the ^{14}N−^{1}H HMQC experiment), so as to be in the same format as the ^{14}N−^{1}H spectra presented in Figure 8a and 8b. A short REDOR[112] recoupling time of one rotor period was used such that predominantly only one-bond correlations are observed, i.e., peaks are observed for the NH and NH$_2$ groups. The resolution is reduced in the ^{1}H dimension as compared to the ^{14}N−^{1}H spectra due to the lower MAS frequency, with this being particularly evident for the NH$_2$ group, where distinct resonances are not resolved for the NH2a and NH2b protons. By contrast, the absence of anisotropic second-order quadrupolar broadening for the spin I = 1/2 ^{15}N nucleus allows resolution of two peaks for the two distinct NH sites. Note also the different shift range in the ^{14}N and ^{15}N spectra due to additional large (up to 200 ppm) isotropic second-order quadrupolar shifts that depend on the quadrupolar coupling constant, i.e., the center of gravity of a ^{14}N line shape depends on the isotropic chemical shift and the isotropic second-order quadrupolar shift (see section S3 in the Supporting Information). This explains why the relative position of the NH and NH$_2$ resonances for **2** have changed in the ^{14}N−^{1}H spectra as compared to the ^{1}H−^{15}N spectrum.

Structural Characterization of G(C3)$_3$ (3), G(C10)$_3$ (4), 8BrG(C10)$_3$ (5), and GaceC10 (6). The above sections have

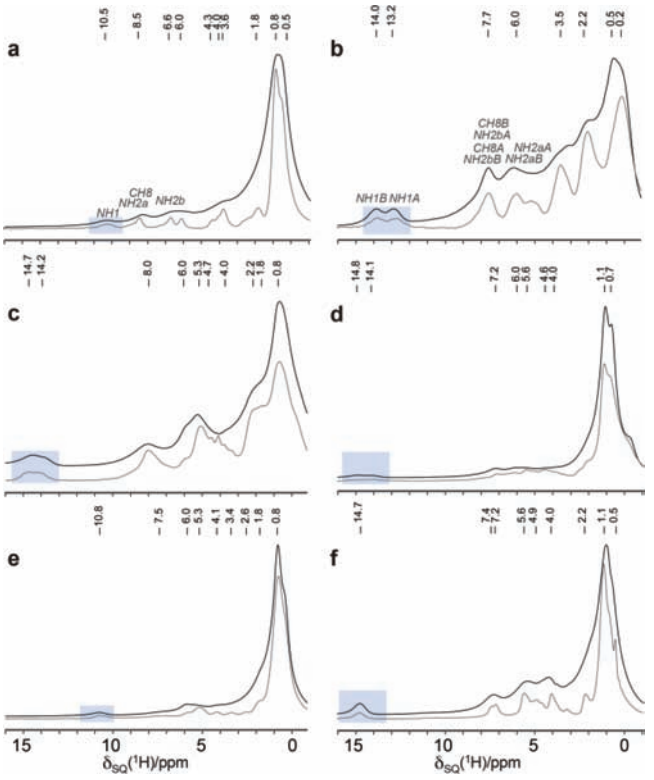

Figure 10. ^{1}H (600 MHz) NMR spectra of (a) **1**, (b) **2**, (c) **3**, (d) **4**, (e) **5**, and (f) **6**. Fast MAS (30 kHz) and homonuclear (DUMBO) decoupled (12 kHz MAS) spectra are shown as black and gray lines, respectively. Highlighted spectral regions correspond to the hydrogen-bonded NH resonances. Chemical shift values for resolved peaks in the DUMBO spectra are indicated. Assignments of the NH, NH_2, and CH8 resonances are labeled for **1** and **2** (see Table 1).

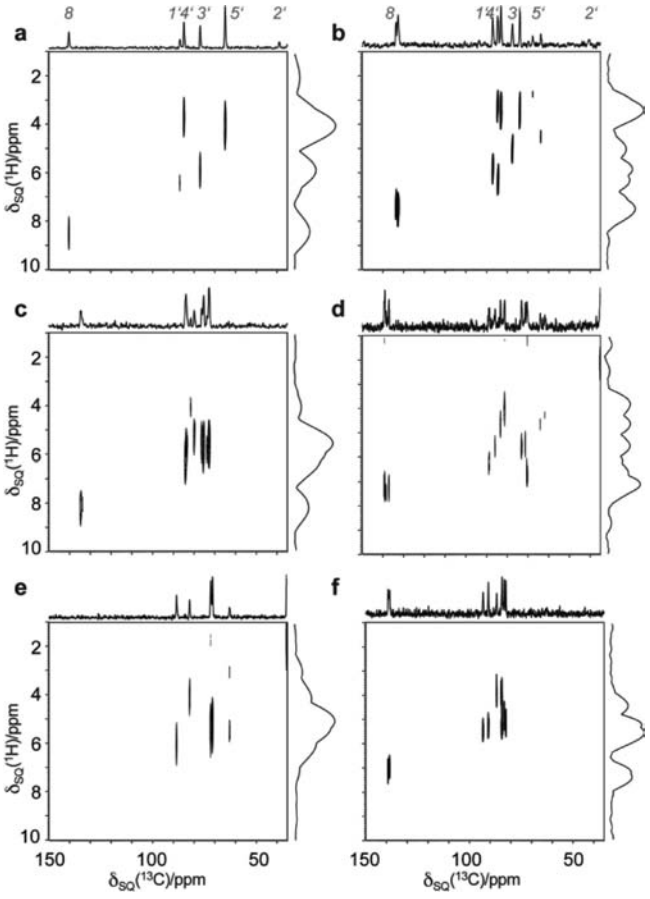

Figure 11. ^{1}H (600 MHz, DUMBO)−^{13}C refocused INEPT spectra of (a) **1**, (b) **2**, (c) **3**, (d) **4**, (e) **5**, and (f) **6**, recorded at 12.5 kHz MAS, together with skyline projections. Expanded regions corresponding to the sugar and CH8 resonances are shown. Assignments are indicated for **1** and **2**, as listed in Table 1. Base contour level is at (a) 9%, (b) 15%, (c) 14%, (d) 6%, (e) 4%, and (f) 18% of the maximum peak height in each spectrum, and negative contours are shown in red.

presented ^{13}C and ^{1}H solid-state NMR spectra obtained at natural abundance for **1** and **2**, which are known from ^{15}N refocused INADEQUATE solid-state NMR spectra recorded for ^{15}N-labeled samples of **1** and **2** to exhibit ribbon-like or quartet-like self-assembly (see Figure 1).[68] In the following, analogous ^{13}C and ^{1}H solid-state NMR spectra, also obtained at natural abundance, are presented for **3**, **4**, **5**, and **6**, for which no single-crystal diffraction structures are available. It will be shown how comparison to spectral fingerprints observed for **1** and **2** allow identification of ribbon-like or quartet-like self-assembly.

^{13}C CP MAS NMR of G(C3)$_3$ (3), G(C10)$_3$ (4), 8BrG(C10)$_3$ (5), and GaceC10 (6). Figure 9 presents ^{13}C CP MAS spectra for **1**−**6**, showing the ^{13}C resonances of the sugar ring sites and the guanine C5 and C8 sites (the other regions of the ^{13}C CP MAS spectra are shown in Figure S5 in the Supporting Information), where the peaks for **1** (Figure 9a) and **2** (Figure 9b) have been assigned above. Note that the derivatives **3**−**6** are not deoxygenated derivatives, i.e., at the C2′ position of the sugar ring there is an oxygen atom, linked to a substituent, which is either an alkanoyl chain identical to that at C3′ (**3** to **5**) or an isopropylidene group joining the oxygen atoms directly bonded to the C2′ and C3′ sites (**6**). Thus, none of the four ^{13}C CP MAS spectra shown in Figures 9c−f contain ^{13}C resonances at approximately 40 ppm, where the CH_2 C2′ site appears in Figure 9a and 9b, with the peak for this site now appearing at approximately 70 ppm, i.e., in a similar position as C3′.

Notably, only Figure 9a and 9e displays one ^{13}C peak per atomic site, which immediately suggests that only **5** assembles to form quartet-like structures in the solid state as in the case of **1**. Moreover, for the sugar region, the spectra in Figure 9c and 9d for **3** and **4** are similar and have many features in common with the spectrum in Figure 9b for the established ribbon structure of **2**. Also in common with **2**, the ^{13}C chemical shifts of the C8 resonances of **3**, **5**, and **6** all appear below 140 ppm. Note that the 8-bromine substitution in **5** shifts this peak the furthest upfield to generate a low-intensity broader resonance around 125 ppm; the broadening is assigned to the known dipolar−quadrupolar cross terms that arise here due to the dipolar coupling to the ^{79}Br (50.5%) or ^{81}Br (49.5%) nucleus (both spin $I = 3/2$).

^{1}H Solid-State NMR of G(C3)$_3$ (3), G(C10)$_3$ (4), 8BrG(C10)$_3$ (5), and GaceC10 (6). A comparison of ^{1}H fast-MAS (30 kHz, black) and CRAMPS (12.5 kHz MAS with DUMBO decoupling, gray) NMR spectra is given in Figure 10 for compounds **1**−**6**. With the line narrowing provided in the ^{1}H CRAMPS spectra it is possible to resolve further ^{1}H peaks as compared to under MAS alone. The multiple CH_2 resonances of the three long alkyl chains in **4** and **5** gives rise to an intense peak at ∼1.0 ppm, which reduces the relative intensity of the higher ppm resonances. Most notably, the hydrogen-bonded NH1 ^{1}H chemical shifts (highlighted in blue) are centered at 10.8 ppm for **5** and between 14.0 and 15.0 ppm for **3**, **4**, and **6**. By analogy with the ^{1}H

Table 3. ^{13}C Experimental Chemical Shifts[a] of CH8 and Sugar Carbon Atoms for the Guanosine Derivatives

site		$\delta(^{13}C)$/ppm **1**	$\delta(^{13}C)$/ppm **2**	$\delta(^{13}C)$/ppm **3**	$\delta(^{13}C)$/ppm **4**	$\delta(^{13}C)$/ppm **5**	$\delta(^{13}C)$/ppm **6**
CH8	A	140.4	132.9	136.8	139.2	125.6	139.3
	B		134.3	134.7	137.1		138.8
CH1′	A	86.7	87.0	84.0	88.8	88.4	93.5
	B		84.5	83.8	86.4		91.0
CH4′	A	84.9	84.5	81.5	83.4	82.1	87.1
	B		83.1	79.9	81.3		84.5
CH3′	A	77.0	77.5	76.4	73.1	72.0	84.5
	B		73.9	75.3	71.3		83.4
CH5′	A	64.9	63.7	64.5	64.1	62.8	64.3
	B		63.7	63.1	61.7		62.8
CH2′	A	39.0	42.7	73.8	70.5	71.1	83.4
	B		40.2	72.7	70.2		82.6

[a] Solid-state NMR chemical shifts as determined from ^{13}C CP MAS (Figures 2 and 9) and ^{1}H (DUMBO)−^{13}C refocused INEPT (Figures 4 and 10) spectra. For **3**, **4**, **5**, and **6**, the assignment of the CH2′ and CH3′ chemical shifts is arbitrary, as is the assignment to the two distinct molecules for **3**, **4**, and **6**.

Table 4. ^{1}H Experimental Chemical Shifts[a] of NH, NH_2, CH8, and Sugar Hydrogen Atoms for the Guanosine Derivatives

site		$\delta(^{1}H)$/ppm **1**	$\delta(^{1}H)$/ppm **2**	$\delta(^{1}H)$/ppm **3**	$\delta(^{1}H)$/ppm **4**	$\delta(^{1}H)$/ppm **5**	$\delta(^{1}H)$/ppm **6**
NH1	A	10.5	13.2	14.7	14.8	10.8	14.7
	B		14.0	14.2	14.1		14.7
NH2a	A	8.5	5.6	5.3	5.4	7.5	5.6
	B		6.1		6.0		
NH2b	A	6.8	7.5	8.6	6.4	6.1	7.4
	B		8.0	8.4	6.8		
CH8	A	8.7	7.7	8.0	7.4		7.2
	B		7.5	8.2	7.2		7.0
CH1′	A	6.6	6.0	6.3	6.2	6.0	5.5
	B		6.2	6.0	5.6		5.3
CH4′	A	3.6	3.5	4.0	4.7	4.1	4.3
	B		3.3	5.3	4.0		4.0
CH3′	A	6.0	5.2	5.5	5.6	5.3	5.2
	B		3.5	5.6	5.5		4.0
CH5′a	A	4.3	4.8	5.3	4.6	5.5	
	B		3.5	4.4	4.3	3.0	
CH5′b	A		3.0	4.7			
	B		3.7				
CH2′a	A	4.0	2.2	5.8	6.6	5.1	4.9
	B		1.4	5.5	6.8		5.2
CH2′b	A	2.2	2.2				3.7
	B		3.5				

[a] Solid-state NMR chemical shifts as determined from ^{1}H (DUMBO)−^{13}C refocused INEPT (Figures 4 and 10) and ^{1}H−^{1}H DQ-SQ (Figures 5, 6, and 12) spectra. For **3**, **4**, **5**, and **6**, the assignment of the CH2′ and CH3′ chemical shifts is arbitrary, as is the assignment to the two distinct molecules for **3**, **4**, and **6**.

chemical shifts of **1** and **2**, this further suggests that **5** exhibits a quartet-like self-assembly driven by N1H···N7 hydrogen bonds as compared to a ribbon-like self-assembly driven by N1H···O6 hydrogen bonds.

^{1}H−^{13}C SQ-SQ Refocused INEPT and ^{1}H−^{1}H DQ-SQ CRAMPS 2D NMR Spectra of G(C3)$_3$ (3), G(C10)$_3$ (4), 8BrG-(C10)$_3$ (5), and GaceC10 (6). Expanded regions of ^{1}H−^{13}C heteronuclear correlation spectra corresponding to the sugar and CH8 resonances are shown in Figure 11 for **3**, **4**, **5**, and **6**. The spectra were recorded using the same pulse sequence and similar experimental conditions to the spectra presented for **1** and **2** in Figure 4; the corresponding regions of these spectra are also presented in Figure 11 for direct comparison.

As discussed above, short (<1.5 ms) $\tau = \tau'$ periods (with eDUMBO$_{22}$ homonuclear decoupling[89]) were used for the refocused INEPT transfer, such that correlation peaks are observed only for directly bonded pairs of ^{13}C−^{1}H nuclei. Correlations peaks are weak or not visible at the contour level shown for the ^{1}H resonances of the CH5′ CH_2 groups. Comparing the ^{1}H−^{13}C SQ-SQ refocused INEPT spectra in Figure 11 for **3**, **4**, **5**, and **6**, the doubling of

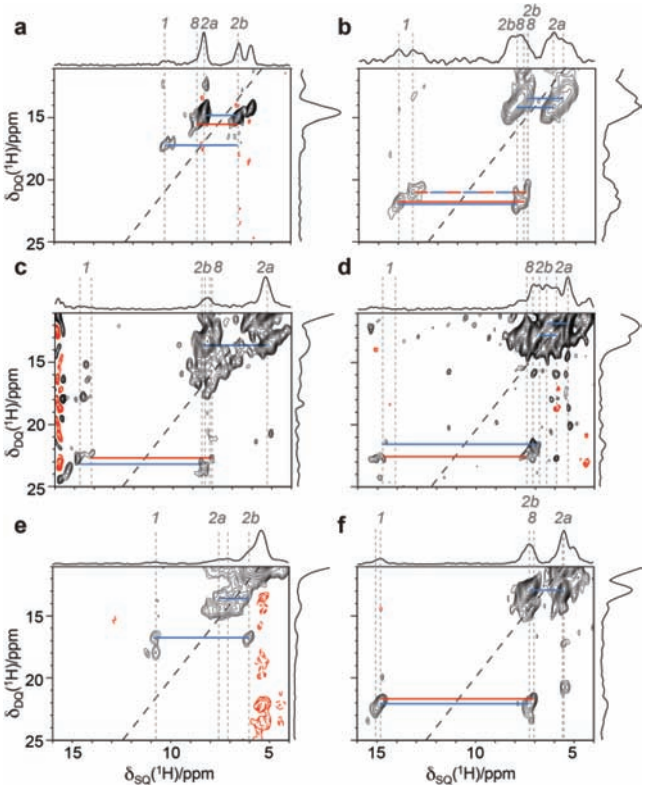

Figure 12. ^{1}H−^{1}H DQ-SQ CRAMPS (DUMBO) spectra of (a) **1**, (b) **2**, (c) **3**, (d) **4**, (e) **5**, and (f) **6**, recorded at 12.5 kHz MAS, together with skyline projections. Expanded regions corresponding to those in Figures 5d and 6d are presented, which show DQ peaks for the NH, NH_2 and CH8 protons. In all spectra, the $F_1 = 2F_2$ diagonal is shown as a black dashed line. Blue and red bars highlight DQ coherences arising from pairs of intra- and intermolecular ^{1}H−^{1}H nuclei, respectively, as discussed in the text. The base contour level is at (a) 1%, (b) 2%, (c) 3%, (d) 1%, (e) 1%, and (f) 1% of the maximum peak height in each spectrum, and negative contours are shown in red.

the resonances per distinct carbon atom is evident for **3**, **4**, and **6**. The spectra also allow the resolution and assignment of the sugar and CH8 ^{1}H resonances (Tables 3 and 4); see discussion below of syn and anti configurations of the sugar ring.

Expanded regions of ^{1}H−^{1}H DQ-SQ CRAMPS spectra corresponding to the NH, NH_2, and CH8 resonances are shown in Figure 12 for **3**, **4**, **5**, and **6**. The spectra were recorded using the same pulse sequence and experimental conditions to the spectra presented for **1** and **2** in Figures 5 and 6; the corresponding regions of these spectra are also presented in Figure 12 for direct comparison. It was noted above that the hydrogen-bonded NH1 ^{1}H chemical shifts of 10.8 ppm for **5** and between 14.0 and 15.0 ppm for **3**, **4**, and **6** suggest, by analogy with the ^{1}H chemical shifts of **1** and **2**, that **5** exhibits a quartet-like self-assembly driven by N1H···N7 hydrogen bonds as compared to a ribbon-like self-assembly driven by N1H···O6 hydrogen bonds. This is further supported by the evident similarity in the pattern of DQ peaks between **1** and **5** and between **2**, **3**, **4**, and **6**. Notably, as observed for **1** and **2**, the relative magnitude of the NH_2, NH2a, and NH2b chemical shifts is also interchanged, i.e., the NH_2 proton closest to the NH proton has the bigger ^{1}H chemical shift for **3**, **4**, and **6** (ribbon-like self-assembly) but the smaller ^{1}H chemical shift for **5** (quartet-like self-assembly). As for Figures 5d and 6d above, blue and red bars highlight DQ coherences arising

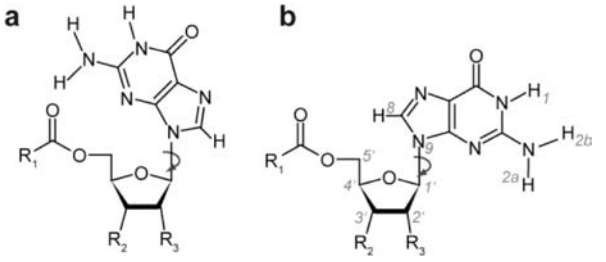

Figure 13. Rotation around the C1′−N9 bond leads to (a) syn and (b) anti conformations.

from pairs of intra- and intermolecular ^{1}H−^{1}H nuclei, respectively. Rows extracted at the highlighted ^{1}H DQ frequencies from the ^{1}H−^{1}H DQ (DUMBO)-SQ (DUMBO) CRAMPS spectra (see Figures 5d and 6d) are shown in Figure S4, Supporting Information.

For the guanosine derivatives studied here, the solid-state ^{1}H chemical shift of the guanine NH group is observed to change from 11 ppm in **1** and **5** to 13−15 ppm in **2**, **3**, **4**, and **6**, corresponding to a change from NH···O to NH···N intermolecular hydrogen bonding. In the literature, there are a number of examples of ^{1}H solid-state NMR chemical shifts over 10 ppm determined for NH moieties that participate in inter- or intramolecular NH···O or NH···N hydrogen bonds, for example, for L-histidine·HCl·H_2O,[93,113,114] bilirubin,[115] ureido−pyrimidinone compounds,[116−118] imidazole-based compounds,[119−125] a discotic trisamide,[120] methylnitroacetanilide,[126] melamine orthophosphate,[127] uracil,[128] a barbituric acid derivative,[129] organosilicas derivatized with purine−pyrimidine base pairs and a ureido−pyrimidinone,[130,131] triazole-functionalized siloxane polymers,[132] 5-fluorouracil and thymine solid solutions,[133] didanosine,[134] ciprofloxacin,[135] the salt formed between quinidine and 4-hydroxybenzoic acid,[136] and bipyridine diamine derivatized discotics.[137] Furthermore, Sharif et al. presented a systematic investigation of a series of 1:1 complexes of aldenamine and aldimine Schiff bases with carboxylic acids that show that the ^{1}H NH chemical shift increases as the N···O hydrogen-bonding distances decreases, i.e., as the hydrogen bond becomes stronger.[138] This is in agreement with a DFT investigation for methylnitroacetanilide dimers.[126] Moreover, the effect of intermolecular hydrogen bonding on ^{1}H chemical shifts has been investigated by comparing chemical shift calculations for the full crystal structure to those for isolated molecules: similar values of up to 6 ppm were determined for NH···O hydrogen bonding in L-histidine·HCl·H_2O,[114] NH···O hydrogen bonding in uracil,[128] and NH···N hydrogen bonding in campho[2,3-*c*]pyrazole.[80] This shows that the change in the solid-state ^{1}H chemical shift of the guanine NH group from 11 ppm in **1** and **5** to 13−15 ppm in **2**, **3**, **4**, and **6** is not simply because the hydrogen-bond acceptor atom has changed from oxygen to nitrogen but rather that the hydrogen bond has become stronger, corresponding to a shorter NH···X hydrogen-bonding distance.

Sugar Conformation: Insight from ^{1}H and ^{13}C Chemical Shifts. Rotation around the C1′−N9 bond is possible to give either a syn or an anti arrangement of the base with respect to the sugar ring (see Figure 13). For the well-organized supramolecular assemblies of stacked quartets formed by **1** in the presence of metal ions (at different relative concentrations) in solution, both syn and anti conformers are observed, with no interconversion on the time scale of solution-state NMR experiments being observed.[6,7] For the single-crystal X-ray diffraction structure of the 5′-Me_2-*t*-BuSi-2′,3′,-di-*O*-isopropylidene derivative that

Table 5. ^{1}H and ^{13}C Solution-State ($CDCl_3$) NMR Chemical Shifts of Syn and Anti Conformers of Quartets of 1 Compared to Solid-State NMR Chemical Shifts of 1 and 5

site	$\delta(^{13}C/^{1}H)$ ppm $\mathbf{1}_8$, KI syn[a]	$\delta(^{13}C/^{1}H)$ ppm $\mathbf{1}_8$, KI anti[a]	$\delta(^{13}C/^{1}H)$ ppm $\mathbf{1}_4$, KPic syn[b]	$\delta(^{13}C/^{1}H)$ ppm $\mathbf{1}_4$, KPic syn[b]	$\delta(^{13}C/^{1}H)$ ppm $\mathbf{1}_4$, KPic anti[b]	$\delta(^{13}C/^{1}H)$ ppm $\mathbf{1}$[c]	$\delta(^{13}C/^{1}H)$ ppm $\mathbf{5}$[d]
CH8	137.7	134.9	139.5	141.1	134.5	140.4	125.6
CH1′	86.6	82.4	85.6	86.7	82.2	86.7	88.4
H8	7.4	8.0	7.6	7.7	7.6	8.7	
H1′	6.2	6.4	6.4	6.1	6.2	6.6	6.0
H2′a	3.6	3.1	2.9	3.6	2.7	4.0	5.1
H2′b	2.4	2.6	2.2	2.6	2.4	2.2	

[a] Solution-state NMR chemical shifts from ref 6. [b] Solution-state NMR chemical shifts from ref 7. [c] See Table 1. [d] See Tables 3 and 4.

exhibits a stacking of quartets, stabilized by K^+ and Cs^+ ions, only syn conformers are present.[12] These observations are interesting since it is the anti conformer that is usually observed to predominate in solid-state structures of nucleosides.[139]

Table 5 compares the ^{1}H and ^{13}C chemical shifts of selected sites for the separate syn and anti conformers observed in solution-state NMR experiments of **1** in the presence of metal ions.[6,7] It is evident that the CH8 and CH1′ ^{13}C chemical shifts are significantly different for the syn and anti conformers with in both cases a larger value being indicative of a syn conformation. For other resonances (^{1}H and ^{13}C), no clear trend is evident. Table 5 further compares these solution-state NMR chemical shifts with the solid-state NMR chemical shifts of **1** and **5**. The CH1′ ^{13}C chemical shift in both cases and the CH8 ^{13}C chemical shift for **1** (the CH8 ^{13}C chemical shift is very different for **5** due to the substituted bromine atom) is indicative of a syn conformation. In this respect, note that a large substituent at the C8 position is known to favor adoption of a syn conformation.[139]

CONCLUSIONS

This paper has shown that ^{1}H solid-state NMR spectroscopy enables the mode of self-assembly adopted by synthetic guanosine derivatives to be identified. In particular, the ^{1}H chemical shift is very sensitive to the different intermolecular hydrogen-bonding arrangements associated with ribbon-like or quartet-like self-assembly. Moreover, ^{1}H DQ spectra are a rich source of information concerning proton−proton proximities, with the enhanced resolution of the ^{1}H DQ CRAMPS experiment enabling intra- and intermolecular proximities involving the alkyl and sugar ring protons as well as the hydrogen-bonded protons to be identified. In this way, the ^{1}H DQ CRAMPS solid-state NMR experiment provides analogous information to the ^{1}H NOE and NOESY experiments in solution-state NMR, the latter having, for example, been used to distinguish between two types of ribbon-like self-assembly adopted by guanosine derivatives by means of observing specific NOEs between sugar and NH_2 protons.[32,33] Importantly, the spectra presented in this paper were obtained for guanosine derivatives at natural abundance, i.e., the mode of self-assembly can be identified without recourse to isotopic labeling, as was the case in our previous work that presented ^{15}N refocused INADEQUATE spectra of ^{15}N-labeled guanosine derivatives.[68]

While the ingenuity of the chemist is leading to the synthesis of guanosine derivatives that self-assemble into a wide range of nanostructures with a diverse range of demonstrated and potential applications, there is a paucity of solid-state atomic-level characterization, with crystal structures having been published for only a few short chain derivatives. Therefore, the ability of solid-state NMR to identify the mode of self-assembly for guanosine derivatives for which it is not possible to obtain single crystals suitable for diffraction structures is of much importance. As noted above in the discussion of Figure 2, it is interesting that narrower ^{13}C line widths are observed in CPMAS spectra for the longer chain derivative **1** as compared to the shorter chain derivative **2**, with a single-crystal X-ray diffraction structure only existing for **2**. Such solid-state characterization is a prerequisite for a better understanding of the factors that control self-assembly and is complementary to the insight obtained from an analysis of two-dimensional structures adopted on surfaces or by solution-state NMR. Indeed, it is known that **1** has a preference for a different ribbon-like structure in $CDCl_3$ solution as compared to that found in the published X-ray single-crystal structure of **2**.[32,33] Moreover, the ^{15}N refocused INADEQUATE spectrum of ^{15}N-labeled **1** unambiguously shows quartet-like formation in the solid state in the absence of metal ions,[68] while only ribbon-like self-assembly is observed in solution. In this way, a solid-state analysis has the advantage that there is not the complication of competing dynamic interactions with solvent molecules, e.g., recent studies have shown that different quartet self-assembly is observed in solution by changing the solvent[24] or the anion.[26] Solid-state analysis does, though, need to carefully investigate polymorphism exhibited as a function of changing crystallization procedures, e.g., from a different solvent.

In conclusion, advanced two-dimensional solid-state NMR spectra are a rich source of atomic-level information on the three-dimensional packing of organic molecules in the solid state. As well as high-resolution ^{1}H experiments, this paper has also illustrated the potential of $^{14}N-^{1}H$ experiments to directly probe NH and NH_2 hydrogen-bonding moieties,[105] with such experiments as demonstrated here for **2** being enabled by access to high magnetic field (850 MHz) and very fast MAS (60 kHz). Such a so-called NMR crystallography[140] approach as presented here for guanosine derivatives has much wider relevance, with many other potential applications to, e.g., other supramolecular structures and pharmaceuticals.

EXPERIMENTAL AND COMPUTATIONAL SECTION

3′,5′-*O*-Didecanoyl 2′-Deoxyguanosine (1). **1** was synthesized as described in ref 68 (compound **2**), starting from isotopically unlabeled deoxyguanosine hydrate (Fluka), and recrystallized from EtOH.

3′,5′-*O*-Dipropanoyl Deoxyguanosine (2). **2** was synthesized as described in ref 141 (compound **3**) and recrystallized from a THF/H_2O (3:2) mixture.

2′,3′,5′-*O*-Tripropanoylguanosine (3). Guanosine (Fluka; 1.0 mmol) was dried over P_2O_5 in vacuo (50 °C, 2 h) and then suspended in MeCN (15 mL). Redistilled Et_3N (4.0 mmol), DMAP (0.16 mmol), and propanoic anhydride (3.4 mmol) were added, and the resulting

mixture was stirred overnight at room temperature. MeOH (0.5 mL) was then added, and stirring was continued for 20 min. The crude was concentrated in vacuo; the residue was suspended in Millipore water and filtered. The precipitate was thoroughly washed with Millipore water and dried in vacuo, affording 0.87 mmol of the title compound as a white solid. The product was recrystallized from EtOH. ^{1}H NMR (DMSO-d_6, 400 MHz): δ 10.72 (bs, 1H, NH), 7.91 (s, 1H, H8), 6.52 (bs, 2H, NH_2), 5.98 (d, J = 6.0 Hz, 1H, H_1'), 5.80 (t, J = 6.0 Hz, 1H, H_2'), 5.52 (dd, J = 6.0 Hz, J = 4.0 Hz,, 1H, H_3'), 4.38−4.29 (m, 3H, H_4', H_5', H_5''), 2.46−2.27 (m, 6H, 3 $-CH_2CO-$), 1.08−0.96 (m, 9H, 3 $-CH_3$) ppm. ^{13}C NMR (DMSO-d_6, 75 MHz): δ 9.67 (CH_3), 9.78 (CH_3), 9.80 (CH_3), 27.31 (CH_2), 27.50 (CH_2), 27.56 (CH_2), 63.96 (5′ CH_2), 71.19 (3′ CH), 73.01 (2′ CH), 80.55 (4′ CH), 85.46 (1′ CH), 117.77 (C), 136.48 (CH), 152.01 (C), 154.80 (C), 157.54 (C), 173.43 (C), 173.56 (C), 174.27 (C) ppm. Anal. Calcd for $C_{19}H_{25}N_5O_8$: C, 50.55; H, 5.58; N, 15.51. Found: C, 50.65; H, 5.58; N, 15.55.

2′,3′,5′-*O*-Tridecanoylguanosine (4). **4** was synthesized as described in ref 73 and recrystallized from EtOH.

8-Bromo-2′,3′,5′-*O*-tridecanoylguanosine (5). **5** was synthesized as described in ref 40 (compound **8**) and recrystallized from EtOH.

2′,3′-*O*-Isopropylidene-5′-decanoylguanosine (6). **6** was synthesized as described in ref 33 (compound **5**) and recrystallized from EtOH.

Solid-State NMR. Except where otherwise stated, experiments were performed on a Bruker Avance II+ spectrometer operating at a ^{1}H Larmor frequency of 600 MHz using a 4 mm triple-resonance probe, operating in double-resonance mode, at a MAS frequency of 12.5 kHz MAS. Except where otherwise stated, the ^{1}H 90° pulse was of duration 2.5 μs. For homonuclear and heteronuclear ^{1}H decoupling, the nutation frequency, ν_1, was equal to 100 kHz. Where ^{13}C FIDs were recorded, TPPM[142] ^{1}H heteronuclear decoupling with a phase shift of 15° was employed (unless otherwise stated). In homonuclear decoupling experiments, windowless eDUMBO-1_{22}[89] or windowed DUMBO-1 (wDUMBO-1)[143,144] sequences were applied during periods of free precession (t_1 and τ, τ' for refocused INEPT) or CRAMPS acquisition in t_2, respectively. Unless otherwise stated, the homonuclear decoupling cycles were of duration 24 μs (320 steps of 75 ns each). For acquisition, a detection window was inserted after each DUMBO-1 cycle to give an effective t_2 dwell time (including prepulses of duration 0.7 μs) of 29.8 μs. Except where otherwise stated, the ^{13}C 90° pulse was of duration 4.0 μs.

^{13}C CP MAS. ^{13}C magnetization was generated by cross-polarization with a ramp[145,146] of (**1**, **5**) 80−100%, (**2**) 50−100%, or (**3**, **4**, **6**) 40−100% on the ^{1}H channel for a contact time of 1 ms. The TPPM ^{1}H heteronuclear decoupling pulse duration was (**1**) 4.9, (**2**, **5**) 4.8, or (**3**, **4**, **6**) 4.7 μs. ^{13}C CP MAS spectra for **3**, **4**, and **6** were recorded on a Varian/Chemagnetics Infinity+ spectrometer operating at a ^{1}H Larmor frequency of 300 MHz using a double-resonance 4 mm probe at 8.5 kHz MAS, while those for **1**, **2**, and **5** were recorded on a Chemagnetics Infinity spectrometer operating at a ^{1}H Larmor frequency of 600 MHz using a 4 mm probe at 8 kHz MAS. There were (**1**) 256, (**2**) 1024, (**3**) 19 200, (**4**) 22 800, (**5**) 512, or (**6**) 20 400 transients coadded, with a recycle delay of (**1**) 2, (**2**) 6, (**3**, **4**, **6**) 3, or (**5**) 2.5 s.

^{1}H fast MAS one-pulse and 2D DQ MAS experiments were performed using a 2.5 mm double-resonance probe at 30 kHz MAS: For one-pulse experiments, (**1**, **2**, **3**) 4 or (**4**, **5**, **6**) 16 transients were coadded, with a recycle delay of (**1**, **2**) 2 or (**3**, **4**, **5**, **6**) 3 s. For DQ MAS experiments,[84] one rotor period of the BABA recoupling sequence[92,147] ($90_x - \tau - 90_{-x}\, 90_y - \tau - 90_{-y}$, where $\tau = \tau_R/2$ minus the pulse durations) was used for excitation and reconversion of DQ coherence. A 16-step phase cycle was used to select $\Delta p = \pm 2$ on the DQ excitation pulses (4 steps) and $\Delta p = -1$ (4 steps) on the z-filter 90° pulse, where p is the coherence order. The recycle delay was 2 s. For each of 128 t_1 FIDs (using the States method to achieve sign discrimination in F_1 with a rotor-synchronized increment of 33 μs), 16 transients were coadded, corresponding to a total experimental time of 1 h.

^{1}H 1D CRAMPS. For a total acquisition time of 11.7 ms, (**1**, **2**) 32 or (**3**, **4**, **5**, **6**) 128 transients were coadded with a recycle delay of 3 s. The scaling factor in F_2 was (**1**, **3**) 0.55 or (**2**, **4**, **5**, **6**) 0.57.

^{1}H 2D DQ CRAMPS. The pulse sequence employed is detailed in ref 94. The same 16-step phase cycle as for the DQ MAS experiment was used. Three basic POST-C7[148] elements (total duration 68.6 μs, ν_1 = 87.5 kHz) were used for excitation and reconversion of DQ coherence. Small prepulses, θ_1 = (**1**, **4**, **6**) 0.75, (**2**, **5**) 0.7, or (**3**) 0.8 μs and θ_2 = (**1**, **4**, **6**) 0.75, (**2**, **5**) 0.7, or (**3**) 0.9 μs, rotate the magnetization from a plane perpendicular to the effective decoupling field to the detection plane (x,y). For a total acquisition time of (**1**) 10.5, (**2**, **6**) 10.7, (**3**, **4**) 7.2, or (**5**) 11.1 ms and for each of 100 t_1 FIDs (using the States-TPPI method to achieve sign discrimination in F_1 with a increment of 48 μs), (**3**) 32 or (otherwise) 16 transients were coadded with a recycle delay of 2.5 s corresponding to a total experimental time of (**3**) 2 or (otherwise) 1 h. The scaling factors were (**1**) 0.60, (**2**, **3**, **6**) 0.61, (**4**) 0.62, or (**5**) 0.64 in F_1 and (**1**, **2**, **3**) 0.55, (**4**, **6**) 0.56, or (**5**) 0.58 in F_2.

^{1}H−^{13}C Refocused INEPT. The pulse sequence and 16-step phase cycle employed is detailed in ref 88. An evolution period, $\tau = \tau'$, of (**1**) 0.64, (**2**) 1.44, (**3**, **6**) 1.28, or (**4**, **5**) 0.96 ms was used. The TPPM ^{1}H heteronuclear decoupling pulse duration was 4.85 μs. For windowless eDUMBO-1_{22}, the homonuclear decoupling cycles were of duration 32 μs (320 steps of 100 ns each). Prepulses of duration 0.5 μs were used. The scaling factor in F_1 was (**1**, **2**) 0.50, (**3**, **4**) 0.58, (**5**) 0.51, or (**6**) 0.62. For each of 60 t_1 slices (using the States-TPPI method to achieve sign discrimination in F_1 with an increment of 64 μs), (**1**, **5**) 512, (**2**, **3**) 576, (**4**) 416, or (**6**) 432 transients were coadded with a recycle delay of 2 s (total experimental time of (**1**, **5**) 17, (**2**, **3**) 19, or (**4**, **6**) 14 h).

^{1}H (DQ-DUMBO)−^{13}C SQ Refocused INEPT. The pulse sequence and 64-step phase cycle employed is detailed in ref 91. The experiment was performed on a Bruker Avance III 850 spectrometer, operating at Larmor frequencies of 850.2 MHz for ^{1}H and 213.7 MHz for ^{13}C using a 3.2 mm triple-resonance probe (operating in double-resonance mode). ^{13}C 90° pulses were of duration 5 μs, and an evolution period, $\tau = \tau'$, of 1.28 ms was used. SPINAL-64 ^{1}H heteronuclear decoupling[149] with a pulse duration of 4.86 μs was used. For windowless eDUMBO-1_{22}, the homonuclear decoupling cycles were of duration 32 μs (320 steps of 100 ns each). Prepulses of duration θ_1 = 1.0 μs were used. The scaling factor in F_1 was 0.61. For each of 112 t_1 FIDs (using the States method to achieve sign discrimination in F_1 with an increment of 64 μs), 1280 transients were coadded with a recycle delay of 2 s (total experimental time of 80 h).

^{14}N−^{1}H HMQC. A modified version of the pulse sequence as shown in Figure 3 of ref 107 was employed, applying a second ^{1}H 90° pulse (90° out of phase with respect to the first 90° pulse) immediately after the first ^{1}H 90° pulse and using $x\ -x$ phase inversion (every rotor period) of the $n = 2$ ($\nu_1 = 2\,\nu_R$) rotary-resonance recoupling pulses.[150] A 4-step nested phase cycle was used to select changes in coherence order $\Delta p = \pm 1$ (on the first ^{1}H pulse, 2 steps) and $\Delta p = \pm 1$ (on the last ^{14}N pulse, 2 steps). Experiments were performed on a Bruker Avance III 850 spectrometer, operating at Larmor frequencies of 850.2 MHz for ^{1}H and 61.4 MHz for ^{14}N using a 1.3 mm triple-resonance probe (operating in double-resonance mode) at a MAS frequency of 60.0 kHz MAS. The ^{1}H and ^{14}N 90° pulse durations were 1.3 and 2 μs, respectively. For each of 36 or 60 t_1 FIDs (using the States method to achieve sign discrimination in F_1 with a rotor-synchronized increment of 16.7 μs), 80 or 240 transients were coadded with a recycle delay of 2 s corresponding to a total experimental time of 100 min or 8 h (parameters are stated for the spectra in Figure 8a and 8c).

^{1}H−^{15}N REPT HSQC. The pulse sequence employed is shown in Figure 3 of ref 111. A 16-step nested phase cycle was used to select changes in coherence order $\Delta p = \pm 1$ (on the first ^{1}H pulse, 2 steps), ± 1 (on the first ^{13}C pulse, 2 steps), and ± 2 (on the first ^{13}C 180° pulse, 4 steps).

The experiment was performed on a Chemagnetics Infinity spectrometer operating at a ^{1}H Larmor frequency of 600 MHz using a 3.2 mm triple-resonance probe, operating in double-resonance mode, at a MAS frequency of 22.0 kHz MAS. Application of the sequence was preceded by a pulse comb on the ^{15}N channel. XiX ^{1}H decoupling[151,152] with a pulse duration of 9 μs was applied during acquisition of the ^{15}N FID. For each of 128 t_1 FIDs (using the TPPI method to achieve sign discrimination in F_1 with a rotor-synchronized increment of 45.5 μs), 80 transients were coadded with a recycle delay of 5 s corresponding to a total experimental time of 14 h.

^{13}C and ^{1}H chemical shifts are referenced with respect to neat TMS using adamantane as a secondary reference (38.5 ppm for the higher ppm ^{13}C resonance[153] and 1.63 ppm for ^{1}H). ^{15}N/^{14}N chemical shifts are referenced relative to neat liquid CH_3NO_2 using the ^{15}N resonance of glycine at −347.4 ppm or the ^{14}N resonance of NH_4Cl (aqueous solution) at −352.9 ppm as an external reference.[154] To convert to the chemical shift scale frequently used in protein NMR, where the reference is liquid ammonia at −50 °C, it is necessary to add 379.5 to the given values.

First-principles NMR Chemical Shielding Calculations. First-principles NMR chemical shielding calculations were performed using the academic release version 4.3 of the CASTEP[155] software package, which implements density functional theory (DFT) within a generalized gradient approximation and the planewave pseudopotential approach. All calculations used the PBE exchange-correlation functional[156] and "ultrasoft" pseudopotentials.[157] Geometry optimization was performed starting with the X-ray diffraction crystal structure of **2** (obtained from the CSD database, refcode MOFBUE,[33] $R = 0.054$ for 13006 observed reflections, $Z = 2$, i.e., 96 atoms in the unit cell). Geometry optimization of all atoms was carried out, resulting in average forces of 0.0046 (C), 0.0043 (N), 0.0038 (O), and 0.0037 (H) eV/Å. Note that distances stated in this paper are for this geometry optimized crystal structure: comparing the database crystal structure with the geometrically optimized structure, the root-mean squared deviation was 0.148 Å for all atoms. The NMR chemical shifts were computed using the gauge-including projector augmented-wave (GIPAW) method.[75,76] For both the geometry optimization and the NMR chemical shielding calculation, a maximum planewave cutoff energy of 800 eV and a Monkhorst-Pack grid of minimum sample spacing 0.08 A^{-1} was used. Calculations were performed using 32 nodes of the University of Warwick Centre for Scientific Computing cluster of 3 GHz Intel Xeon 5160 processors taking 8.5 and 3.5 h for the geometry optimization and the NMR chemical shielding calculations, respectively.

X-ray Powder Diffraction. Data were collected using a Bruker D8 diffractometer in Debye−Scherrer geometry, employing a copper anode with the generator set at 40 kV, 40 mA. The incident beam was monochromated to Kα_1. A point detector was used. The sample was contained in a 0.7 mm Lindemann glass capillary, which was spun about its axis during data collection. Data were collected in the angular range 2−60° 2-theta at a 0.02° increment. Due to the weak X-ray scattering from the sample, data were collected over a total of 42 h.

■ ASSOCIATED CONTENT

Supporting Information. Comparison of experimental and calculated NMR chemical shifts for **2**; GIPAW calculated chemical shift tensors for **2**; GIPAW calculated electric field gradients for **2**; further tables and analysis of ^{1}H DQ correlation peaks; H−N proximities in **2**; experimental chemical shifts for guanosine derivatives **3**-**6**; powder X-ray diffraction results for **1** (pdf); geometry-optimized (CASTEP) structure for **2** (pdb file). This material is available free of charge via the Internet at http://pubs.acs.org.

■ AUTHOR INFORMATION

Corresponding Author

S.P.Brown@warwick.ac.uk

Present Addresses

[‖]Université de Lyon, Centre de RMN à très hauts champs, CNRS/ENS Lyon/UCBL, 5 rue de la Doua, 69100 Villeurbanne, France.

[⊥]Chemical Development, Analytical Sciences, GlaxoSmithKline PLC, Gunnels Wood Road, Stevenage, SG1 2NY, United Kingdom.

Funding Sources

Funding from EPSRC and GSK (United Kingdom) and University of Bologna (Italy) is acknowledged. The U.K. 850 MHz solid-state NMR Facility used in this research was funded by EPSRC and BBSRC as well as the University of Warwick including partial funding through Birmingham Science City Advanced Materials Projects 1 and 2 supported by Advantage West Midlands (AWM) and the European Regional Development Fund (ERDF).

■ ACKNOWLEDGMENT

CASTEP calculations were performed on the University of Warwick Centre for Scientific Computing cluster. We are grateful to Accelrys for providing the Materials Studio Interface. Helpful discussions with Stephen Wimperis, Luminita Duma, Hans Forster, and Stefan Steuernagel concerning ^{14}N−^{1}H experiments and with Jonathan Yates concerning GIPAW calculations are acknowledged. We gratefully acknowledge the European Commission through the COST Action MP0802 (Self-assembled guanosine structures for molecular electronic devices) for offering a stimulating environment for highly qualified discussions on the topic.

■ REFERENCES

(1) Davis, J. T. *Angew. Chem., Int. Ed. Engl.* **2004**, *43*, 668.
(2) Davis, J. T.; Spada, G. P. *Chem. Soc. Rev.* **2007**, *36*, 296.
(3) Lena, S.; Masiero, S.; Pieraccini, S.; Spada, G. P. *Chem.—Eur. J.* **2009**, *15*, 7792.
(4) Gottarelli, G.; Masiero, S.; Spada, G. P. *J. Chem. Soc., Chem. Commun.* **1995**, 2555.
(5) Davis, J. T.; Tirumala, S.; Jenssen, J. R.; Radler, E.; Fabris, D. *J. Org. Chem.* **1995**, *60*, 4167.
(6) Marlow, A. L.; Mezzina, E.; Spada, G. P.; Masiero, S.; Davis, J. T.; Gottarelli, G. *J. Org. Chem.* **1999**, *64*, 5116.
(7) Mezzina, E.; Mariani, P.; Itri, R.; Masiero, S.; Pieraccini, S.; Spada, G. P.; Spinozzi, F.; Davis, J. T.; Gottarelli, G. *Chem.—Eur. J.* **2001**, *7*, 388.
(8) Kaucher, M. S.; Lam, Y. F.; Pieraccini, S.; Gottarelli, G.; Davis, J. T. *Chem.—Eur. J.* **2005**, *11*, 164.
(9) Evan-Salem, T.; Frish, L.; van Leeuwen, F. W. B.; Reinhoudt, D. N.; Verboom, W.; Kaucher, M. S.; Davis, J. T.; Cohen, Y. *Chem.—Eur. J.* **2007**, *13*, 1969.
(10) Martic, S.; Liu, X. Y.; Wang, S. N.; Wu, G. *Chem.—Eur. J.* **2008**, *14*, 1196.
(11) Ma, L.; Iezzi, M.; Kaucher, M. S.; Lam, Y. F.; Davis, J. T. *J. Am. Chem. Soc.* **2006**, *128*, 15269.
(12) Forman, S. L.; Fettinger, J. C.; Pieraccini, S.; Gottarelli, G.; Davis, J. T. *J. Am. Chem. Soc.* **2000**, *122*, 4060.
(13) Kotch, F. W.; Fettinger, J. C.; Davis, J. T. *Org. Lett.* **2000**, *2*, 3277.
(14) Shi, X. D.; Fettinger, J. C.; Davis, J. T. *J. Am. Chem. Soc.* **2001**, *123*, 6738.
(15) Shi, X. D.; Fettinger, J. C.; Davis, J. T. *Angew. Chem., Int. Ed. Engl.* **2001**, *40*, 2827.
(16) Shi, X. D.; Mullaugh, K. M.; Fettinger, J. C.; Jiang, Y.; Hofstadler, S. A.; Davis, J. T. *J. Am. Chem. Soc.* **2003**, *125*, 10830.
(17) Wong, A.; Fettinger, J. C.; Forman, S. L.; Davis, J. T.; Wu, G. *J. Am. Chem. Soc.* **2002**, *124*, 742.

(18) Wu, G.; Wong, A.; Gan, Z. H.; Davis, J. T. *J. Am. Chem. Soc.* **2003**, *125*, 7182.
(19) Ida, R.; Wu, G. *Chem. Commun.* **2005**, 4294.
(20) Wong, A.; Kotch, F. W.; Kwan, I. C. M.; Davis, J. T.; Wu, G. *Chem. Commun.* **2009**, 2154.
(21) Cai, M.; Marlow, A. L.; Fettinger, J. C.; Fabris, D.; Haverlock, T. J.; Moyer, B. A.; Davis, J. T. *Angew. Chem., Int. Ed. Engl.* **2000**, *39*, 1283.
(22) Shi, X. D.; Fettinger, J. C.; Cai, M. M.; Davis, J. T. *Angew. Chem., Int. Ed. Engl.* **2000**, *39*, 3124.
(23) Garcia-Arriaga, M.; Hobley, G.; Rivera, J. M. *J. Am. Chem. Soc.* **2008**, *130*, 10492.
(24) Betancourt, J. E.; Martin-Hidalgo, M.; Gubala, V.; Rivera, J. M. *J. Am. Chem. Soc.* **2009**, *131*, 3186.
(25) Rivera-Sanchez, M. D.; Andujar-de-Sanctis, I.; Garcia-Arriaga, M.; Gubala, V.; Hobley, G.; Rivera, J. M. *J. Am. Chem. Soc.* **2009**, *131*, 10403.
(26) Gonzalez-Rodriguez, D.; van Dongen, J. L. J.; Lutz, M.; Spek, A. L.; Schenning, A.; Meijer, E. W. *Nat. Chem.* **2009**, *1*, 151.
(27) Kotch, F. W.; Sidorov, V.; Lam, Y. F.; Kayser, K. J.; Li, H.; Kaucher, M. S.; Davis, J. T. *J. Am. Chem. Soc.* **2003**, *125*, 15140.
(28) van Leeuwen, F. W. B.; Verboom, W.; Shi, X. D.; Davis, J. T.; Reinhoudt, D. N. *J. Am. Chem. Soc.* **2004**, *126*, 16575.
(29) Sreenivasachary, N.; Lehn, J. M. *Proc. Natl. Acad. Sci. U. S. A.* **2005**, *102*, 5938.
(30) Gottarelli, G.; Masiero, S.; Mezzina, E.; Spada, G. P.; Mariani, P.; Recanatini, M. *Helv. Chim. Acta* **1998**, *81*, 2078.
(31) Gottarelli, G.; Masiero, S.; Mezzina, E.; Pieraccini, S.; Spada, G. P.; Mariani, P. *Liq. Cryst.* **1999**, *26*, 965.
(32) Gottarelli, G.; Masiero, S.; Mezzina, E.; Pieraccini, S.; Rabe, J. P.; Samori, P.; Spada, G. P. *Chem.—Eur. J.* **2000**, *6*, 3242.
(33) Giorgi, T.; Grepioni, F.; Manet, I.; Mariani, P.; Masiero, S.; Mezzina, E.; Pieraccini, S.; Saturni, L.; Spada, G. P.; Gottarelli, G. *Chem.—Eur. J.* **2002**, *8*, 2143.
(34) Thewalt, U.; Bugg, C. E.; Marsh, R. E. *Acta Crystallogr., Sect. B* **1970**, *26*, 1089.
(35) Araki, K.; Takasawa, R.; Yoshikawa, I. *Chem. Commun.* **2001**, 1826.
(36) Sato, T.; Seko, M.; Takasawa, R.; Yoshikawa, I.; Araki, K. *J. Mater. Chem.* **2001**, *11*, 3018.
(37) Yoshikawa, I.; Li, J.; Sakata, Y.; Araki, K. *Angew. Chem., Int. Ed. Engl.* **2004**, *43*, 100.
(38) Yoshikawa, I.; Sawayama, J.; Araki, K. *Angew. Chem., Int. Ed. Engl.* **2008**, *47*, 1038.
(39) Sessler, J. L.; Sathiosatham, M.; Doerr, K.; Lynch, V.; Abboud, K. A. *Angew. Chem., Int. Ed. Engl.* **2000**, *39*, 1356.
(40) Giorgi, T.; Lena, S.; Mariani, P.; Cremonini, M. A.; Masiero, S.; Pieraccini, S.; Rabe, J. P.; Samori, P.; Spada, G. P.; Gottarelli, G. *J. Am. Chem. Soc.* **2003**, *125*, 14741.
(41) Lena, S.; Cremonini, M. A.; Federiconi, F.; Gottarelli, G.; Graziano, C.; Laghi, L.; Mariani, P.; Masiero, S.; Pieraccini, S.; Spada, G. P. *Chem.—Eur. J.* **2007**, *13*, 3441.
(42) Lena, S.; Brancolini, G.; Gottarelli, G.; Mariani, P.; Masiero, S.; Venturini, A.; Palermo, V.; Pandoli, O.; Pieraccini, S.; Samori, P.; Spada, G. P. *Chem.—Eur. J.* **2007**, *13*, 3757.
(43) Kumar, A. M. S.; Fox, J. D.; Buerkle, L. E.; Marchant, R. E.; Rowan, S. J. *Langmuir* **2009**, *25*, 653.
(44) Nikan, M.; Sherman, J. C. *Angew. Chem., Int. Ed. Engl.* **2008**, *47*, 4900.
(45) Sidorov, V.; Kotch, F. W.; El-Khouedi, M.; Davis, J. T. *Chem. Commun.* **2000**, 2369.
(46) Zhong, C.; Wang, J.; Wu, N. Q.; Wu, G.; Zavalij, P. Y.; Shi, X. D. *Chem. Commun.* **2007**, 3148.
(47) Arnal-Herault, C.; Pasc, A.; Michau, M.; Cot, D.; Petit, E.; Barboiu, M. *Angew. Chem., Int. Ed. Engl.* **2007**, *46*, 8409.
(48) Likhitsup, A.; Yu, S.; Ng, Y. H.; Chai, C. L. L.; Tam, E. K. W. *Chem. Commun.* **2009**, 4070.
(49) Mihai, S.; Cazacu, A.; Arnal-Herault, C.; Nasr, G.; Meffre, A.; van der Lee, A.; Barboiu, M. *New J. Chem.* **2009**, *33*, 2335.
(50) Kaucher, M. S.; Harrell, W. A.; Davis, J. T. *J. Am. Chem. Soc.* **2006**, *128*, 38.
(51) Ma, L.; Melegari, M.; Colombini, M.; Davis, J. T. *J. Am. Chem. Soc.* **2008**, *130*, 2938.
(52) Ma, L.; Harrell, W. A.; Davis, J. T. *Org. Lett.* **2009**, *11*, 1599.
(53) Rinaldi, R.; Branca, E.; Cingolani, R.; Masiero, S.; Spada, G. P.; Gottarelli, G. *Appl. Phys. Lett.* **2001**, *78*, 3541.
(54) Maruccio, G.; Visconti, P.; Arima, V.; D'Amico, S.; Blasco, A.; D'Amone, E.; Cingolani, R.; Rinaldi, R.; Masiero, S.; Giorgi, T.; Gottarelli, G. *Nano Lett.* **2003**, *3*, 479.
(55) Rinaldi, R.; Maruccio, G.; Biasco, A.; Arima, V.; Cingolani, R.; Giorgi, T.; Masiero, S.; Spada, G. P.; Gottarelli, G. *Nanotechnology* **2002**, *13*, 398.
(56) Neogi, A.; Li, J.; Neogi, P. B.; Sarkar, A.; Moroc, H. *Electron. Lett.* **2004**, *40*, 1605.
(57) Liddar, H.; Li, J.; Neogi, A.; Neogi, P. B.; Sarkar, A.; Cho, S.; Morkoc, H. *Appl. Phys. Lett.* **2008**, *92*, 013309.
(58) Ghoussoub, A.; Lehn, J. M. *Chem. Commun.* **2005**, 5763.
(59) Pieraccini, S.; Masiero, S.; Pandoli, O.; Samori, P.; Spada, G. P. *Org. Lett.* **2006**, *8*, 3125.
(60) Graziano, C.; Masiero, S.; Pieraccini, S.; Lucarini, M.; Spada, G. P. *Org. Lett.* **2008**, *10*, 1739.
(61) Neviani, P.; Mileo, E.; Masiero, S.; Pieraccini, S.; Lucarini, M.; Spada, G. P. *Org. Lett.* **2009**, *11*, 3004.
(62) Spada, G. P.; Lena, S.; Masiero, S.; Pieraccini, S.; Surin, M.; Samori, P. *Adv. Mater.* **2008**, *20*, 2433.
(63) Pieraccini, S.; Bonacchi, S.; Lena, S.; Masiero, S.; Montalti, M.; Zaccheroni, N.; Spada, G. P. *Org. Biomol. Chem.* **2010**, *8*, 774.
(64) Lena, S.; Neviani, P.; Masiero, S.; Pieraccini, S.; Spada, G. P. *Angew. Chem., Int. Ed. Engl.* **2010**, *49*, 3657.
(65) Lesage, A.; Bardet, M.; Emsley, L. *J. Am. Chem. Soc.* **1999**, *121*, 10987.
(66) Fayon, F.; Massiot, D.; Levitt, M. H.; Titman, J. J.; Gregory, D. H.; Duma, L.; Emsley, L.; Brown, S. P. *J. Chem. Phys.* **2005**, *122*, 194313.
(67) Cadars, S.; Sein, J.; Duma, L.; Lesage, A.; Pham, T. N.; Baltisberger, J. H.; Brown, S. P.; Emsley, L. *J. Magn. Reson.* **2007**, *188*, 24.
(68) Pham, T. N.; Masiero, S.; Gottarelli, G.; Brown, S. P. *J. Am. Chem. Soc.* **2005**, *127*, 16018.
(69) Brown, S. P.; Perez-Torralba, M.; Sanz, D.; Claramunt, R. M.; Emsley, L. *J. Am. Chem. Soc.* **2002**, *124*, 1152.
(70) Brown, S. P.; Perez-Torralba, M.; Sanz, D.; Claramunt, R. M.; Emsley, L. *Chem. Commun.* **2002**, 1852.
(71) Pham, T. N.; Griffin, J. M.; Masiero, S.; Lena, S.; Gottarelli, G.; Hodgkinson, P.; Fillip, C.; Brown, S. P. *Phys. Chem. Chem. Phys.* **2007**, *9*, 3416.
(72) Claramunt, R. M.; Perez-Torralba, M.; Santa Maria, D.; Sanz, D.; Elena, B.; Alkorta, I.; Elguero, J. *J. Magn. Reson.* **2010**, *206*, 274.
(73) Devetak, M.; Masiero, S.; Pieraccini, S.; Spada, G. P.; Copic, M.; Olenik, I. D. *Appl. Surf. Sci.* **2010**, *256*, 2038.
(74) Harris, R. K. *Analyst* **2006**, *131*, 351.
(75) Pickard, C. J.; Mauri, F. *Phys. Rev. B* **2001**, *63*, 245101.
(76) Yates, J. R.; Pickard, C. J.; Mauri, F. *Phys. Rev. B* **2007**, *76*, 024401.
(77) www.gipaw.net.
(78) Harris, R. K.; Hodgkinson, P.; Pickard, C. J.; Yates, J. R.; Zorin, V. *Magn. Reson. Chem.* **2007**, *45*, S174.
(79) Johnston, J. C.; Iuliucci, R. J.; Facelli, J. C.; Fitzgerald, G.; Mueller, K. T. *J. Chem. Phys.* **2009**, *131*, 144503.
(80) Webber, A. L.; Emsley, L.; Claramunt, R. M.; Brown, S. P. *J. Phys. Chem. A* **2010**, *114*, 10435.
(81) Schnell, I.; Brown, S. P.; Low, H. Y.; Ishida, H.; Spiess, H. W. *J. Am. Chem. Soc.* **1998**, *120*, 11784.
(82) Brown, S. P.; Schnell, I.; Brand, J. D.; Mullen, K.; Spiess, H. W. *J. Am. Chem. Soc.* **1999**, *121*, 6712.
(83) Zorin, V. E.; Brown, S. P.; Hodgkinson, P. *J. Chem. Phys.* **2006**, *125*, 144508.
(84) Brown, S. P. *Prog. Nucl. Magn. Reson. Spectrosc.* **2007**, *50*, 199.

(85) Madhu, P. K. *Solid State Nucl. Magn. Reson.* **2009**, *35*, 2.
(86) Lesage, A. *Phys. Chem. Chem. Phys.* **2009**, *11*, 6876.
(87) Hodgkinson, P. *Annu. Rep. NMR Spectrosc.* **2011**, *72*, 185.
(88) Elena, B.; Lesage, A.; Steuernagel, S.; Bockmann, A.; Emsley, L. *J. Am. Chem. Soc.* **2005**, *127*, 17296.
(89) Elena, B.; de Paepe, G.; Emsley, L. *Chem. Phys. Lett.* **2004**, *398*, 532.
(90) Yates, J. R.; Pham, T. N.; Pickard, C. J.; Mauri, F.; Amado, A. M.; Gil, A. M.; Brown, S. P. *J. Am. Chem. Soc.* **2005**, *127*, 10216.
(91) Webber, A. L.; Elena, B.; Griffin, J. M.; Yates, J. R.; Pham, T. N.; Mauri, F.; Pickard, C. J.; Gil, A. M.; Stein, R.; Lesage, A.; Emsley, L.; Brown, S. P. *Phys. Chem. Chem. Phys.* **2010**, *12*, 6970.
(92) Schnell, I.; Lupulescu, A.; Hafner, S.; Demco, D. E.; Spiess, H. W. *J. Magn. Reson.* **1998**, *133*, 61.
(93) Madhu, P. K.; Vinogradov, E.; Vega, S. *Chem. Phys. Lett.* **2004**, *394*, 423.
(94) Brown, S. P.; Lesage, A.; Elena, B.; Emsley, L. *J. Am. Chem. Soc.* **2004**, *126*, 13230.
(95) Mifsud, N.; Elena, B.; Pickard, C. J.; Lesage, A.; Emsley, L. *Phys. Chem. Chem. Phys.* **2006**, *8*, 3418.
(96) Avenier, P.; Taoufik, M.; Lesage, A.; Solans-Monfort, X.; Baudouin, A.; de Mallmann, A.; Veyre, L.; Basset, J. M.; Eisenstein, O.; Emsley, L.; Quadrelli, E. A. *Science* **2007**, *317*, 1056.
(97) Avenier, P.; Lesage, A.; Taoufik, M.; Baudouin, A.; De Mallmann, A.; Fiddy, S.; Vautier, M.; Veyre, L.; Basset, J. M.; Emsley, L.; Quadrelli, E. A. *J. Am. Chem. Soc.* **2007**, *129*, 176.
(98) Griffin, J. M.; Martin, D. R.; Brown, S. P. *Angew. Chem., Int. Ed. Engl.* **2007**, *46*, 8036.
(99) Salager, E.; Stein, R. S.; Pickard, C. J.; Elena, B.; Emsley, L. *Phys. Chem. Chem. Phys.* **2009**, *11*, 2610.
(100) Mafra, L.; Gomes, J. R. B.; Trebosc, J.; Rocha, J.; Amoureux, J. P. *J. Magn. Reson.* **2009**, *196*, 88.
(101) Mafra, L.; Siegel, R.; Fernandez, C.; Schneider, D.; Aussenac, F.; Rocha, J. *J. Magn. Reson.* **2009**, *199*, 111.
(102) Brown, S. P.; Spiess, H. W. *Chem. Rev.* **2001**, *101*, 4125.
(103) Brown, S. P. *Macromol. Rapid Commun.* **2009**, *30*, 688.
(104) Ciesielski, A.; Lena, S.; Masiero, S.; Spada, G. P.; Samori, P. *Angew. Chem., Int. Ed. Engl.* **2010**, *49*, 1963.
(105) Cavadini, S. *Prog. Nucl. Magn. Reson. Spectrosc.* **2010**, *56*, 46.
(106) Cavadini, S.; Antonijevic, S.; Lupulescu, A.; Bodenhausen, G. *J. Magn. Reson.* **2006**, *182*, 168.
(107) Gan, Z. H.; Amoureux, J. P.; Trebosc, J. *Chem. Phys. Lett.* **2007**, *435*, 163.
(108) Nishiyama, Y.; Endo, Y.; Nemoto, T.; Utsumi, H.; Yamauchi, K.; Hioka, K.; Asakura, T. *J. Magn. Reson.* **2011**, *208*, 44.
(109) Oas, T. G.; Griffin, R. G.; Levitt, M. H. *J. Chem. Phys.* **1988**, *89*, 692.
(110) Veshtort, M.; Griffin, R. G. *J. Magn. Reson.* **2006**, *178*, 248.
(111) Saalwachter, K.; Graf, R.; Spiess, H. W. *J. Magn. Reson.* **2001**, *148*, 398.
(112) Gullion, T.; Schaefer, J. *J. Magn. Reson.* **1989**, *81*, 196.
(113) Gu, Z. T.; Ridenour, C. F.; Bronnimann, C. E.; Iwashita, T.; McDermott, A. *J. Am. Chem. Soc.* **1996**, *118*, 822.
(114) Schmidt, J.; Hoffmann, A.; Spiess, H. W.; Sebastiani, D. *J. Phys. Chem. B* **2006**, *110*, 23204.
(115) Brown, S. P.; Zhu, X. X.; Saalwachter, K.; Spiess, H. W. *J. Am. Chem. Soc.* **2001**, *123*, 4275.
(116) Schnell, I.; Langer, B.; Sontjens, S. H. M.; van Genderen, M. H. P.; Sijbesma, R. P.; Spiess, H. W. *J. Magn. Reson.* **2001**, *150*, 57.
(117) Schnell, I.; Langer, B.; Sontjens, S. H. M.; Sijbesma, R. P.; van Genderen, M. H. P.; Spiess, H. W. *Phys. Chem. Chem. Phys.* **2002**, *4*, 3750.
(118) Armstrong, G.; Alonso, B.; Massiot, D.; Buggy, M. *Magn. Reson. Chem.* **2005**, *43*, 405.
(119) Goward, G. R.; Schuster, M. F. H.; Sebastiani, D.; Schnell, I.; Spiess, H. W. *J. Phys. Chem. B* **2002**, *106*, 9322.
(120) Fischbach, I.; Thieme, K.; Hoffmann, A.; Hehn, M.; Schnell, I. *J. Magn. Reson.* **2003**, *165*, 102.
(121) Benhabbour, S. R.; Chapman, R. P.; Scharfenberger, G.; Meyer, W. H.; Goward, G. R. *Chem. Mater.* **2005**, *17*, 1605.
(122) Traer, J. W.; Montoneri, E.; Samoson, A.; Past, J.; Tuherm, T.; Goward, G. R. *Chem. Mater.* **2006**, *18*, 4747.
(123) Traer, J. W.; Goward, G. R. *Magn. Reson. Chem.* **2007**, *45*, S135.
(124) Traer, J. W.; Britten, J. F.; Goward, G. R. *J. Phys. Chem. B* **2007**, *111*, 5602.
(125) Traer, J. W.; Goward, G. R. *Phys. Chem. Chem. Phys.* **2010**, *12*, 263.
(126) Harris, R. K.; Ghi, P. Y.; Hammond, R. B.; Ma, C. Y.; Roberts, K. J. *Chem. Commun.* **2003**, 2834.
(127) Brinkmann, A.; Litvinov, V. M.; Kentgens, A. P. M. *Magn. Reson. Chem.* **2007**, *45*, S231.
(128) Uldry, A. C.; Griffin, J. M.; Yates, J. R.; Perez-Torralba, M.; Maria, M. D. S.; Webber, A. L.; Beaumont, M. L. L.; Samoson, A.; Claramunt, R. M.; Pickard, C. J.; Brown, S. P. *J. Am. Chem. Soc.* **2008**, *130*, 945.
(129) Bolz, I.; Moon, C.; Enkelmann, V.; Brunklaus, G.; Spange, S. *J. Org. Chem.* **2008**, *73*, 4783.
(130) Arrachart, G.; Carcel, C.; Moreau, J. J. E.; Hartmeyer, G.; Alonso, B.; Massiot, D.; Creff, G.; Bantignies, J. L.; Dieudonne, P.; Man, M. W. C.; Althoff, G.; Babonneau, F.; Bonhomme, C. *J. Mater. Chem.* **2008**, *18*, 392.
(131) Arrachart, G.; Creff, G.; Wadepohl, H.; Blanc, C.; Bonhomme, C.; Babonneau, F.; Alonso, B.; Bantignies, J. L.; Carcel, C.; Moreau, J. J. E.; Dieudonne, P.; Sauvajol, J. L.; Massiot, D.; Man, M. W. C. *Chem.—Eur. J.* **2009**, *15*, 5002.
(132) Akbey, U.; Granados-Focil, S.; Coughlin, E. B.; Graf, R.; Spiess, H. W. *J. Phys. Chem. B* **2009**, *113*, 9151.
(133) Vogt, F. G.; Vena, J. A.; Chavda, M.; Clawson, J. S.; Strohmeier, M.; Barnett, M. E. *J. Mol. Struct.* **2009**, *932*, 16.
(134) Bettini, R.; Menabeni, R.; Tozzi, R.; Pranzo, M. B.; Pasquali, I.; Chierotti, M. R.; Gobetto, R.; Pellegrino, L. *J. Pharm. Sci.* **2010**, *99*, 1855.
(135) Linck, Y. G.; Chattah, A. K.; Graf, R.; Romanuk, C. B.; Olivera, M. E.; Manzo, R. H.; Monti, G. A.; Spiess, H. W. *Phys. Chem. Chem. Phys.* **2011**, *13*, 6590.
(136) Khan, M. K. M.; Enkelmann, V.; Brunklaus, G. *CrystEngComm* **2011**, *13*, 3213.
(137) Metzroth, T.; Hoffmann, A.; Martin-Rapun, R.; Smulders, M. M. J.; Pieterse, K.; Palmans, A. R. A.; Vekemans, J.; Meijer, E. W.; Spiess, H. W.; Gauss, J. *Chem. Sci.* **2011**, *2*, 69.
(138) Sharif, S.; Schagen, D.; Toney, M. D.; Limbach, H. H. *J. Am. Chem. Soc.* **2007**, *129*, 4440.
(139) Saenger, W. *Principles of Nucleic Acid Structure*; Springer: New York, 1984.
(140) In *NMR Crystallography*; Harris, R. K., Wasylishen, R. E., Duer, M. J., Eds.; Wiley: Chichester, 2009.
(141) Manet, I.; Francini, L.; Masiero, S.; Pieraccini, S.; Spada, G. P.; Gottarelli, G. *Helv. Chim. Acta* **2001**, *84*, 2096.
(142) Bennett, A. E.; Rienstra, C. M.; Auger, M.; Lakshmi, K. V.; Griffin, R. G. *J. Chem. Phys.* **1995**, *103*, 6951.
(143) Sakellariou, D.; Lesage, A.; Hodgkinson, P.; Emsley, L. *Chem. Phys. Lett.* **2000**, *319*, 253.
(144) Lesage, A.; Sakellariou, D.; Hediger, S.; Elena, B.; Charmont, P.; Steuernagel, S.; Emsley, L. *J. Magn. Reson.* **2003**, *163*, 105.
(145) Hediger, S.; Meier, B. H.; Kurur, N. D.; Bodenhausen, G.; Ernst, R. R. *Chem. Phys. Lett.* **1994**, *223*, 283.
(146) Metz, G.; Wu, X. L.; Smith, S. O. *J. Magn. Reson., Ser. A* **1994**, *110*, 219.
(147) Sommer, W.; Gottwald, J.; Demco, D. E.; Spiess, H. W. *J. Magn. Reson., Ser. A* **1995**, *113*, 131.
(148) Hohwy, M.; Jakobsen, H. J.; Eden, M.; Levitt, M. H.; Nielsen, N. C. *J. Chem. Phys.* **1998**, *108*, 2686.
(149) Khitrin, A.; Fung, B. M. *J. Chem. Phys.* **2000**, *112*, 2392.
(150) Costa, P. R.; Gross, J. D.; Hong, M.; Griffin, R. G. *Chem. Phys. Lett.* **1997**, *280*, 95.

(151) Tekely, P.; Palmas, P.; Canet, D. *J. Magn. Reson., Ser. A* **1994**, *107*, 129.
(152) Detken, A.; Hardy, E. H.; Ernst, M.; Meier, B. H. *Chem. Phys. Lett.* **2002**, *356*, 298.
(153) Morcombe, C. R.; Zilm, K. W. *J. Magn. Reson.* **2003**, *162*, 479.
(154) Mason, J. In *Encyclopedia of Nuclear Magnetic Resonance*; Grant, D. M., Harris, R. K., Eds.; Wiley: Chichester, U.K., 1996; Vol. 5, p 3222.
(155) Clark, S. J.; Segall, M. D.; Pickard, C. J.; Hasnip, P. J.; Probert, M. J.; Refson, K.; Payne, M. C. *Z. Kristallogr.* **2005**, *220*, 567.
(156) Perdew, J. P.; Burke, K.; Enzernhof, M. *Phys. Rev. Lett.* **1999**, *77*, 3865.
(157) Vanderbilt, D. *Phys. Rev. B* **1990**, *41*, 7892.